

Complete super-sample lensing covariance in the response approach

Alexandre Barreira,¹ Elisabeth Krause,^{2,3} and Fabian Schmidt¹

¹Max-Planck-Institut für Astrophysik, Karl-Schwarzschild-Str. 1, 85741 Garching, Germany

²California Institute of Technology, 1200 E California Blvd, Pasadena, CA 91125, U.S.A.

³Jet Propulsion Laboratory, 4800 Oak Grove Dr, Pasadena, CA 91109, U.S.A.

E-mail: barreira@MPA-Garching.MPG.DE, ekrause@caltech.edu, fabians@MPA-Garching.MPG.DE

Abstract. We derive the complete super-sample covariance (SSC) of the matter and weak lensing convergence power spectra using the power spectrum response formalism to accurately describe the coupling of super-to-intra survey modes. The SSC term is completely characterized by the survey window function, the nonlinear matter power spectrum and the full first-order nonlinear power spectrum response function, which describes the response to super-survey density and tidal field perturbations. Separate universe simulations can efficiently measure these responses in the nonlinear regime of structure formation, which is necessary for lensing applications. Under the Limber and flat-sky approximations, we show that the tidal contributions, which have not been included in cosmological analyses so far, represent a significant fraction ($\approx 20 - 25\%$) of the total SSC, even for an isotropic survey footprint on the sky. The SSC is the dominant off-diagonal contribution to the total lensing covariance for survey sky fractions $f_{\text{sky}} \lesssim 0.3$, making it important to include these tidal terms in cosmic shear analyses.

Contents

1	Introduction	1
2	Power spectrum responses	3
3	Three-dimensional matter power spectrum covariance	6
3.1	Covariance decomposition	6
3.2	The super-sample term with responses	8
4	Lensing covariance	10
4.1	Derivation	10
4.2	Numerical results	12
5	Summary and conclusions	15
A	Derivation of the three-dimensional matter covariance with a finite window	17
B	The super sample term at tree level	18
C	The Limber approximation in the convergence trispectrum	19

1 Introduction

One of the main goals of current and future large-scale structure surveys is to constrain the parameters of cosmological models and infer their overall goodness of fit to the data. Central to this exercise is the likelihood function $\mathcal{L}(\mathbf{D}|\mathbf{M}(\Theta))$, which measures the likelihood that the data vector \mathbf{D} is a realization of a model characterized by a set of parameters Θ , which makes the prediction \mathbf{M} for the data. The inference of the model parameters is then given by the posterior distribution, which according to Bayes' theorem is given by $\mathcal{P}(\Theta|\mathbf{D}) = \mathcal{L}(\mathbf{D}|\mathbf{M}(\Theta))\mathcal{P}(\Theta)/\mathcal{P}(\mathbf{D})$, where $\mathcal{P}(\Theta)$ and $\mathcal{P}(\mathbf{D})$ are called the prior and evidence, respectively. In most real data analyses, the observed data vector \mathbf{D} is assumed to be Gaussian distributed, in which case the likelihood is given by a multivariate Gaussian distribution (see e.g. Refs. [1, 2] for the limitations of this assumption)

$$\mathcal{L}(\mathbf{D}|\mathbf{M}(\Theta)) = \frac{1}{\sqrt{(2\pi)^d \det(\mathbf{Cov})}} \exp \left[-\frac{1}{2} (\mathbf{M}(\Theta) - \mathbf{D})^t \mathbf{Cov}^{-1} (\mathbf{M}(\Theta) - \mathbf{D}) \right]. \quad (1.1)$$

There are three ingredients in this likelihood function. The first is the data vector \mathbf{D} , e.g., a set of estimated galaxy or lensing power spectra in wavenumber bins. Second, we have $\mathbf{M}(\Theta)$, which corresponds to the theoretical model prediction for the ensemble average of the data vector. The final and third piece \mathbf{Cov} is the covariance matrix, which describes the statistical and systematic errors of the analysis. In this paper, we focus on the calculation of the covariance matrix, which is usually far less well understood than the model prediction $\mathbf{M}(\Theta)$, despite its crucial importance for cosmological parameter inference.

The covariance of the three-dimensional matter power spectrum ($\text{Cov}(\mathbf{k}_1, \mathbf{k}_2)$, or matter covariance for short) is the starting point to the evaluation of the covariance of galaxy or lensing two-point statistics, which are what is actually used in real data analyses (e.g. Refs. [3–10]). Given an estimator $\hat{P}_m(\mathbf{k})$ of the matter power spectrum in a wavemode bin centered at \mathbf{k} , the covariance is defined as

$$\begin{aligned}\text{Cov}(\mathbf{k}_1, \mathbf{k}_2) &= \langle \hat{P}(\mathbf{k}_1) \hat{P}(\mathbf{k}_2) \rangle - \langle \hat{P}(\mathbf{k}_1) \rangle \langle \hat{P}(\mathbf{k}_2) \rangle \\ &= \text{Cov}^{\text{G}}(\mathbf{k}_1, \mathbf{k}_2) + \text{Cov}^{\text{cNG}}(\mathbf{k}_1, \mathbf{k}_2) + \text{Cov}^{\text{SSC}}(\mathbf{k}_1, \mathbf{k}_2),\end{aligned}\quad (1.2)$$

where the angle brackets denote ensemble averages. The calculation of the matter covariance can be broken down into the evaluation of three terms (more details will be provided in the sections below). These are (i) the Gaussian (G) covariance, (ii) the connected non-Gaussian (cNG) covariance, and (iii) the super-sample covariance (SSC). During the linear regime of structure formation, and for Gaussian-distributed initial conditions, the diagonal Gaussian covariance is the only contribution. It is straightforwardly given in terms of the power spectrum and is therefore well understood. The cNG term is given by a specific configuration of the matter trispectrum (the Fourier transform of the matter four-point correlation function; cf. Eq. (3.11)) that describes the correlations between observed modes that arise as nonlinear structure formation develops at late times [11–16]. Finally, the SSC term accounts for the correlation between observed modes and modes whose wavelength is larger than the survey size [17–22]. For instance, if the observed region is embedded in a large-scale super-survey overdensity, then structures in the survey have evolved faster compared to the case where the survey is embedded in a region at cosmic mean density; the SSC term describes this uncertainty (the amplitude of the super-survey overdensity could alternatively be regarded as a signal to be fitted for [19]). We note, for completeness, that in addition to these three sample covariance terms, real analyses must also take into account noise in the data as well as systematic errors of the measurement process.

In Ref. [16], the authors have used the power spectrum response formalism [15] to calculate the cNG term. The power spectrum response functions [23–27] describe how the local power spectrum changes as a function of the amplitude of large-scale density and tidal field perturbations. They readily give the squeezed-limit of N -point matter correlation functions, and as a result, can be used to describe the coupling between soft (or long-wavelength) and hard (or short-wavelength) modes in perturbation theory [28]. The shape of these response functions can be evaluated efficiently in the nonlinear regime of structure formation using separate universe simulations [18, 19, 23, 24, 26, 29, 30], thus permitting to describe these soft-to-hard mode couplings in the nonlinear regime of the hard modes (see Ref. [15] for a more formal introduction to the response formalism in large-scale structure). By working up to 1-loop level in perturbation theory, the authors of Ref. [16] demonstrated that the responses capture the total contribution to the cNG covariance when $k_2 \ll k_1$, with $k_2 < k_{\text{NL}}$ and any nonlinear value of k_1 (where k_i denotes the amplitude of the vector mode \mathbf{k}_i), as argued before in Ref. [31]. For general (non-squeezed) configurations of the modes k_1, k_2 , the response-approach calculation is able to reproduce the cNG covariance estimated from large ensembles of simulations (e.g. Ref. [32]) to within 20 – 40%. The usefulness of the response approach in calculations of the matter covariance can ultimately be traced back to the fact that the covariance is dominated by soft-to-hard mode-coupling terms, which are precisely what can be described fully nonlinearly with responses.

In this paper, we turn our attention to the calculation of the SSC term in the response approach. Since it corresponds to the coupling between small-scale modes inside the survey

and long wavelength modes outside, it is amenable to be captured completely by response functions. Indeed, in Ref. [17], the authors invoked the so-called *trispectrum consistency relation* to derive the SSC as the response of the matter power spectrum to the presence of an infinitely long-wavelength isotropic density perturbation. In previous literature, essentially the same contribution was referred to as *beat coupling* [12, 33–35] and *halo sample variance* [36–39]. The SSC term derived in Ref. [17] (and subsequently studied in Refs. [18, 19] using separate universe simulations) has been incorporated in the analysis of recent galaxy and lensing surveys (see e.g. Ref. [9] for a description of the statistical analysis of the DES year 1 results [10]).

Here, we will use the response formalism to rigorously derive and understand the origin of the SSC contributions to the covariance, including tidal contributions not considered in Ref. [17]. Recently, Refs. [40–42] have shown that super-survey tidal fields induce anisotropies (in addition to those induced by redshift-space distortions and the Alcock-Paczyński effect) in the clustering pattern of galaxies. Their derivation made use of a perturbative approach, using the leading-order expressions for the response functions, which is valid only on quasi-linear scales. Here, we focus instead on the impact of the large-scale tidal fields on lensing observables, in particular, on their contribution to the SSC of the two-dimensional lensing convergence power spectrum. By using the separate universe simulation measurements of the matter power spectrum responses, our treatment is valid in the fully nonlinear regime of structure formation. We shall see that the new anisotropic (or tidal) SSC terms can amount to $\approx 20 - 25\%$ of the total SSC contribution, which is itself the dominant off-diagonal contribution to the total covariance. These terms should, as a result, be included in cosmological parameter inference analyses using weak lensing data.

The outline of this paper is as follows. In Sec. 2, we begin by reviewing the basics of the response approach, a specific extension of perturbation theory. In Sec. 3.1, we define the three-dimensional matter covariance in the presence of a finite survey window function and, in Sec. 3.2, we then explicitly use the response approach to derive the full SSC term, which is one of the main results of this paper. In Sec. 4, we derive the covariance matrix of the lensing convergence field and present a few numerical results for an idealized lensing survey. We summarize and conclude in Sec. 5. In Appendix A, we present details about the derivation of the matter covariance for finite surveys; Appendix B provides more intuition about the derivation of the SSC by working at tree-level in perturbation theory; and in Appendix C, we derive in detail the relation between the spectra and trispectra of the two- and three-dimensional density field under the Limber and flat-sky approximations.

2 Power spectrum responses

In this section, we briefly outline the definition of power spectrum responses. We will limit ourselves to laying down the relevant equations and definitions that will be used throughout, and refer the interested reader to Ref. [15] for a more formal derivation. We adopt the diagram rules of cosmological perturbation theory with the conventions listed in Appendix A of Ref. [15]. Further, in our notation $\mathbf{k}_{12\dots n} = \mathbf{k}_1 + \mathbf{k}_2 + \dots + \mathbf{k}_n$ and $k = |\mathbf{k}|$ denotes the amplitude of vector \mathbf{k} .

The n -th order matter power spectrum response \mathcal{R}_n can be defined with the following

interaction vertex

$$\begin{aligned}
& \lim_{\{p_a\} \rightarrow 0} \left(\begin{array}{c} \text{Diagram: A central shaded blob with } n \text{ incoming lines labeled } p_1, \dots, p_n \text{ and two outgoing lines labeled } k' \text{ and } k. \text{ Below the blob is the label } \mathcal{R}_n(k, \dots) P_m(k). \end{array} \right) \\
&= \frac{1}{2} \mathcal{R}_n(k; \{\mu_{\mathbf{k}, \mathbf{p}_a}\}, \{\mu_{\mathbf{p}_a, \mathbf{p}_b}\}, \{p_a/p_b\}) P_m(k) (2\pi)^3 \delta_D(\mathbf{k} + \mathbf{k}' - \mathbf{p}_{1\dots n}). \quad (2.1)
\end{aligned}$$

Physically, it is interpreted as the *response* of the nonlinear power spectrum of the small-scale (hard) mode \mathbf{k} to the presence of n long-wavelength (soft) modes $\mathbf{p}_1, \dots, \mathbf{p}_n$. The dashed blob thus describes the fully evolved nonlinear matter power spectrum $P_m(k)$, as well as all its possible interactions (including loops) with the n long wavelength perturbations. In our notation, $\lim_{\{p_a\} \rightarrow 0}$ means that we keep the leading contribution in the limit in which all soft momenta approach zero. The response \mathcal{R}_n depends on the scale k , as well as on the cosine of the angles between the soft modes involved and their angles with the hard mode \mathbf{k} ; the response does not depend on the absolute value of the soft momenta, but depends on their ratios in general.

With the aid of the diagrammatic representation of the responses, we can establish a link between \mathcal{R}_n and the squeezed limit of the $(n+2)$ -point matter correlation function. Explicitly, if we *attach* propagators (i.e., power spectra) to the soft momentum lines in Eq. (2.1), then we can write

$$\begin{aligned}
& \lim_{\{p_a\} \rightarrow 0} \left(\begin{array}{c} \text{Diagram: Similar to Eq. (2.1) but with each soft mode line } p_a \text{ having a dot at its end, representing an attachment point for a propagator.} \end{array} + (\text{perm.}) \right) = \langle \delta(\mathbf{k}) \delta(\mathbf{k}') \delta(\mathbf{p}_1) \cdots \delta(\mathbf{p}_n) \rangle_{c, \mathcal{R}_n} \\
&= n! \mathcal{R}_n(k; \{\mu_{\mathbf{k}, \mathbf{p}_a}\}, \{\mu_{\mathbf{p}_a, \mathbf{p}_b}\}, \{p_a/p_b\}) P_m(k) \left[\prod_{a=1}^n P_L(p_a) \right] (2\pi)^3 \delta_D(\mathbf{k} + \mathbf{k}' + \mathbf{p}_{1\dots n}), \quad (2.2)
\end{aligned}$$

with the subscript $_c$ denoting connected correlators and the $n!$ factor accounting for the permutations of the \mathbf{p}_a . The subscript \mathcal{R}_n in the $(n+2)$ -connected correlator serves to indicate that only certain contributions to the correlation function are actually captured by \mathcal{R}_n . The remaining contributions to $\langle \delta(\mathbf{k}) \delta(\mathbf{k}') \delta(\mathbf{p}_1) \cdots \delta(\mathbf{p}_n) \rangle_c$ are either small in the squeezed limit, or are response-type terms as well, but described by lower order responses \mathcal{R}_m , $1 \leq m < n$, in conjunction with perturbation theory kernels involving only the soft modes \mathbf{p}_a .

By interpreting the local nonlinear matter power spectrum as a biased tracer of large-scale structure, the \mathcal{R}_n can be expanded in terms of all local gravitational observables (or operators O) associated with the n long-wavelength modes. These operators form a basis \mathcal{K}_O that does not depend on the mode k and that unequivocally specifies the angular structure of \mathcal{R}_n :

$$\mathcal{R}_n(k; \{\mu_{\mathbf{k}, \mathbf{p}_a}\}, \{\mu_{\mathbf{p}_a, \mathbf{p}_b}\}, \{p_a/p_b\}) = \sum_O R_O(k) \mathcal{K}_O^{(n)}(\{\mu_{\mathbf{k}, \mathbf{p}_a}\}, \{\mu_{\mathbf{p}_a, \mathbf{p}_b}\}, \{p_a/p_b\}). \quad (2.3)$$

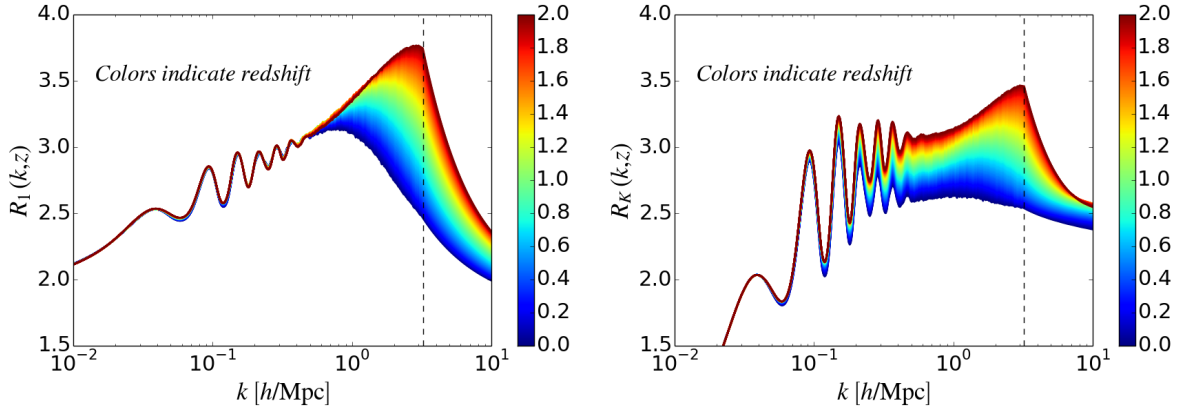


Figure 1. Redshift- and scale-dependence of the R_1 (left) and R_K (right) response coefficients (cf. Eqs. (2.5)). The curves are color coded by redshift. The result shown is obtained via interpolation from the five existing simulation measurements at $z = 0, 0.5, 1, 2, 3$. The simulation results of Ref. [26] measured the response up to $k_N \approx 3.2 h \text{ Mpc}^{-1}$ (dashed vertical line); the result for $k > k_N$ is obtained with the extrapolation of Eq. (2.6).

The functions $R_O(k)$ are called *response coefficients* and their physical interpretation is that they describe the response of the power spectrum to the specific configuration of the large-scale perturbations that each multiplies. At tree level in perturbation theory, the k -dependence of the coefficients can be derived analytically by plugging Eq. (2.3) into Eq. (2.2). In the nonlinear regime of structure formation, these response functions can be evaluated using separate universe simulations that take into account the effects of perturbations larger than the size of the box.

In this paper, we wish to use responses to evaluate the SSC of the matter power spectrum, for which we shall need only the first order case $n = 1$, \mathcal{R}_1 . Up to first order, there are only two operators with associated kernels \mathcal{K}_O , which correspond to a density and a tidal perturbation. Following the notation of Ref. [15] we write

$$\mathcal{R}_1(k, \mu) = R_1(k) + R_K(k) \left(\mu^2 - \frac{1}{3} \right), \quad (2.4)$$

where $\mu = \mathbf{k} \mathbf{p} / p k$. The first-order isotropic response coefficient R_1 has been measured in the nonlinear regime with separate universe simulations in Ref. [18]; in Ref. [26], the higher-order responses R_2 and R_3 were measured as well. Currently, there are no published simulation measurements of the first order response to a tidal field R_K . Here, to make calculations, we shall adopt the extrapolation of the tree-level shape of $R_K(k)$ to the nonlinear regime put forward in Ref. [15]. This was based on the assumption that the modulation of the nonlinear growth by a large-scale tidal field has the same *shape* (as a function of scale k) as that due to a large-scale density perturbation. Effectively, in this paper we take:

$$R_1(k) = 1 - \frac{1}{3} k \frac{P'_m(k)}{P_m(k)} + G_1(k); \quad R_K(k) = \frac{12}{13} G_1(k) - k \frac{P'_m(k)}{P_m(k)}, \quad (2.5)$$

where primes denote derivatives with respect to k , and $G_1(k)$ is the so-called *growth-only response* at first order measured in Ref. [26]. Note that both R_1 and R_K match the tree-level result on large scales. Further, the rescaling contribution $\propto P'_m(k)$ in R_K is a coordinate-transformation effect [43] and exact. Thus, the only possible error in the prediction for

R_K in Eq. (2.5) is in the amplitude of the growth effect $\propto G_1(k)$ on nonlinear scales. The scale and redshift dependence of these two response coefficients is shown in Fig. 1. Strictly, Ref. [26] only ran simulations that allowed to measure the response coefficients at five fixed redshift values, $z = 0, 0.5, 1, 2, 3$; the redshift dependence shown in Fig. 1 is obtained by interpolating over these five measurements. Further, the simulation box used in Ref. [26] ($L_{\text{box}} = 500 \text{ Mpc}/h$ with $N_p = 512^3$ particles) provides measurements of the responses in the range $k \in [k_{\text{fund}}, k_{\text{N}}]$, with $k_{\text{fund}} = 2\pi/L_{\text{box}} \approx 0.012 \text{ h Mpc}^{-1}$ and $k_{\text{N}} = N_p^{1/3}\pi/L_{\text{box}} \approx 3.2 \text{ h Mpc}^{-1}$. However, in the lensing calculations we perform below, we will need to evaluate the responses outside this range. For $k < k_{\text{fund}}$, we take the linear theory result $G_1^{\text{tree}} = 26/21$. For $k > k_{\text{N}}$, we extrapolate the growth-only response as

$$G_1(k > k_{\text{N}}) \longrightarrow G_1(k = k_{\text{N}}) \left(\frac{k}{k_{\text{N}}} \right)^{-1}. \quad (2.6)$$

This is consistent with the physically expected result that the growth-only response approaches zero on small scales since virialization processes inside halos effectively suppress the effect of the large-scale perturbations, i.e., matter density fluctuations on very small scales “lose their memory” of the large-scale environment. The choice of the exponent -1 was chosen to ensure a smooth transition at $k = k_{\text{N}}$, where the simulation-measured $G_1(k)$ approximately shows this scaling with k . As a test, we have verified that our conclusions regarding the relative size of the anisotropic SSC terms do not change if we quite aggressively set $G_1(z, k) = 0$ for $k > k_{\text{N}}$.

3 Three-dimensional matter power spectrum covariance

In this section, we derive the expressions of the covariance of the three-dimensional matter power spectrum in the presence of a finite survey window function, which includes the full SSC term. We will follow closely the notation in Sec. II of Ref. [17] to facilitate comparisons. The content of this section forms the basis for the derivation of the covariance of the lensing power spectrum described in the next section.

3.1 Covariance decomposition

Let us define the matter density contrast field measured inside a survey with window function $W(\mathbf{x})$ as

$$\delta_W(\mathbf{x}) = W(\mathbf{x})\delta(\mathbf{x}), \quad (3.1)$$

where $\delta(\mathbf{x})$ is the three-dimensional matter density contrast and $W(\mathbf{x})$ is unity if \mathbf{x} is inside the observed region and zero otherwise. The Fourier transform of $\delta_W(\mathbf{x})$ is thus given by the convolution of the Fourier transform of the density contrast with the Fourier transform of the window function (tildes indicate Fourier-space quantities)

$$\tilde{\delta}_W(\mathbf{k}) = \int \frac{d^3\mathbf{p}}{(2\pi)^3} \tilde{W}(\mathbf{p}) \tilde{\delta}(\mathbf{k} - \mathbf{p}) \equiv \int_{\mathbf{p}} \tilde{W}(\mathbf{p}) \tilde{\delta}(\mathbf{k} - \mathbf{p}), \quad (3.2)$$

where the second equality serves to define our shorthand notation $\int_{\mathbf{p}}$, which we adopt throughout. We also always assume the continuum limit in Fourier space, which is valid if the modes considered are much larger than the fundamental mode, $k \gg 2\pi/L$, where

$L \sim V_W^{1/3}$ ($V_W = \int d^3\mathbf{x} W(\mathbf{x})$ is the survey volume). We further define the following estimator of the three-dimensional matter power spectrum measured in the survey

$$\hat{P}_W(\mathbf{k}_1) = \frac{1}{V_W} \tilde{\delta}_W(\mathbf{k}_1) \tilde{\delta}_W(-\mathbf{k}_1). \quad (3.3)$$

Note that we allow this estimator to depend on the orientation of \mathbf{k}_1 , i.e., we are not restricting to the case of angle-averaged power spectra as is commonly the case in the literature. The ensemble average of this power spectrum estimator is

$$\begin{aligned} \langle \hat{P}_W(k_1) \rangle &= \frac{1}{V_W} \int_{\mathbf{p}_1} \int_{\mathbf{p}_2} \tilde{W}(\mathbf{p}_1) \tilde{W}(\mathbf{p}_2) \langle \tilde{\delta}(\mathbf{k}_1 - \mathbf{p}_1) \tilde{\delta}(-\mathbf{k}_1 - \mathbf{p}_2) \rangle \\ &= \frac{1}{V_W} \int_{\mathbf{p}} |\tilde{W}(\mathbf{p})|^2 P_m(\mathbf{k} - \mathbf{p}), \end{aligned} \quad (3.4)$$

where we have used the definition of the matter power spectrum $(2\pi)^3 \delta_D(\mathbf{k} + \mathbf{k}') P_m(\mathbf{k}) = \langle \delta(\mathbf{k}) \delta(\mathbf{k}') \rangle$. As mentioned above, we will always consider kinematic regimes in which the modes \mathbf{k} are much larger than the width of the window function in Fourier space, $k \gg 1/L$. Further, noting that for $p \gg 1/L$ the above integral is suppressed by $|W(\mathbf{p})|$, we can approximate $P_m(\mathbf{k} - \mathbf{p}) \approx P_m(\mathbf{k})$ in Eq. (3.4) (i.e. the result is only non-negligible if $k \gg p$). Then, $\langle \hat{P}_W(\mathbf{k}_1) \rangle = P_m(\mathbf{k}) V_W^{-1} \int_{\mathbf{p}} |\tilde{W}(\mathbf{p})|^2 = P_m(\mathbf{k})$, which demonstrates that the above estimator is unbiased for $k \gg p$.

The sample covariance of the estimator of Eq. (3.4) can then be written as

$$\begin{aligned} \text{Cov}(\mathbf{k}_1, \mathbf{k}_2) &= \langle \hat{P}_W(\mathbf{k}_1) \hat{P}_W(\mathbf{k}_2) \rangle - \langle \hat{P}_W(\mathbf{k}_1) \rangle \langle \hat{P}_W(\mathbf{k}_2) \rangle \\ &= \frac{1}{V_W^2} \left[\langle \tilde{\delta}_W(\mathbf{k}_1) \tilde{\delta}_W(\mathbf{k}_2) \rangle \langle \tilde{\delta}_W(-\mathbf{k}_1) \tilde{\delta}_W(-\mathbf{k}_2) \rangle + (\mathbf{k}_2 \leftrightarrow -\mathbf{k}_2) \right] \\ &\quad + \frac{1}{V_W^2} \langle \tilde{\delta}_W(\mathbf{k}_1) \tilde{\delta}_W(-\mathbf{k}_1) \tilde{\delta}_W(\mathbf{k}_2) \tilde{\delta}_W(-\mathbf{k}_2) \rangle_c. \end{aligned} \quad (3.5)$$

In Appendix A, we analyse these correlators with some detail to help understand the impact of the survey window function in the matter covariance. Here, we display directly the final result, which can be written as

$$\begin{aligned} \text{Cov}(\mathbf{k}_1, \mathbf{k}_2) &\equiv \text{Cov}(k_1, k_2, \mu_{12}) = \text{Cov}^G(k_1, k_2, \mu_{12}) + \text{Cov}^{\text{NG}}(k_1, k_2, \mu_{12}) \\ \text{Cov}^G(k_1, k_2, \mu_{12}) &= \frac{1}{V_W^2} [P_m(\mathbf{k}_1)]^2 \left[|\tilde{W}(\mathbf{k}_1 + \mathbf{k}_2)|^2 + |\tilde{W}(\mathbf{k}_1 - \mathbf{k}_2)|^2 \right] \\ \text{Cov}^{\text{NG}}(k_1, k_2, \mu_{12}) &= \frac{1}{V_W^2} \int_{\mathbf{p}} |\tilde{W}(\mathbf{p})|^2 T_m(\mathbf{k}_1, -\mathbf{k}_1 + \mathbf{p}, \mathbf{k}_2, -\mathbf{k}_2 - \mathbf{p}), \end{aligned} \quad (3.6)$$

where $\mu_{12} = \mathbf{k}_1 \mathbf{k}_2 / k_1 / k_2$ and the trispectrum is defined as $(2\pi)^3 \delta_D(\mathbf{k}_{abcd}) T_m(\mathbf{k}_a, \mathbf{k}_b, \mathbf{k}_c, \mathbf{k}_d) = \langle \delta(\mathbf{k}_a) \delta(\mathbf{k}_b) \delta(\mathbf{k}_c) \delta(\mathbf{k}_d) \rangle_c$. The first term on the right-hand side of Eq. (3.6) is the so-called Gaussian (G) part of the covariance, which contributes only if $|\mathbf{k}_1 \pm \mathbf{k}_2| \ll 1/L$; for an infinite volume, the window functions in the Gaussian term effectively work as Dirac-delta functions. Thus, the Gaussian contribution is diagonal. The second, “NG” term involving the trispectrum can be split into the non-Gaussian super-sample covariance (SSC) term that we wish to focus on in this paper, as well as into the connected non-Gaussian (cNG) term. We discuss these non-Gaussian terms in more detail next.

3.2 The super-sample term with responses

The key quantity that sets the non-Gaussian matter covariance is the trispectrum in the configuration that appears in Eq. (3.6). The mode-coupling interactions captured by this configuration of the trispectrum can be described by the following general diagram

$$T_m(\mathbf{k}_1, -\mathbf{k}_1 + \mathbf{p}, \mathbf{k}_2, -\mathbf{k}_2 - \mathbf{p}) = \text{Diagram} \quad , \quad (3.7)$$

where the big empty blob is meant to account for all kinematically allowed vertex and loop interactions, as well as the corresponding connecting propagators, i.e. power spectra. If $p = 0$, the above trispectrum configuration reduces to the standard degenerate configuration of the covariance, i.e., that which corresponds to the case of infinite survey window functions. We can thus define the super sample covariance contribution as that which arises for finite small $p \ll k_1, k_2$ due to large-scale correlations of the modes with wavenumber p , and thus is proportional to $P_L(p)$, i.e.¹

$$T^{\text{SSC}}(\mathbf{k}_1, -\mathbf{k}_1, \mathbf{k}_2, -\mathbf{k}_2; \mathbf{p}) = \left[\lim_{p \rightarrow 0} \frac{\partial}{\partial [P_L(p)]} T_m(\mathbf{k}_1, -\mathbf{k}_1 + \mathbf{p}, \mathbf{k}_2, -\mathbf{k}_2 - \mathbf{p}) \right] P_L(p). \quad (3.9)$$

By inspecting the possible flow of momentum inside the blob in Eq. (3.7), we see that the SSC contribution has to be associated with diagrams in which there is a line (signifying a propagator $P_L(p)$) with momentum \mathbf{p} connecting the left (i.e., $\mathbf{k}_1, -\mathbf{k}_1 + \mathbf{p}$) and the right (i.e., $\mathbf{k}_2, -\mathbf{k}_2 - \mathbf{p}$) sides; this is the only diagram proportional to $P_L(p)$. All other diagrams are, in the limit $p \rightarrow 0$, either (i) independent of p , and thus not of the SSC type (they belong to the connected non-Gaussian contribution); or (ii) depend on higher even powers of p , such as $(p/k_1)^2$. Contributions of this second type are analytic in p and do not involve the large-scale power spectrum $P_L(p)$. They correspond to the smoothing of the trispectrum by the window function, and are thus not considered a part of SSC, in that they do not describe the gravitational coupling between modes of wavenumbers \mathbf{p} and $\mathbf{k}_1, \mathbf{k}_2$. Appendix B illustrates these arguments and provides more intuition about the derivation of the SSC term by working at tree level in perturbation theory.

Recalling that we are considering kinematic cases in which $p \lesssim 1/L \ll k_1, k_2$ (cases with $p > 1/L$ will be suppressed by the window function and cases with $k_1, k_2 \sim 1/L$ are dominated by the Gaussian contribution), then the diagrams contributing to the SSC term defined above correspond to the interaction of a soft mode \mathbf{p} with two hard modes $\mathbf{k}_1, \mathbf{k}_2$, which are two interactions of the \mathcal{R}_1 type. Within the response approach, we can thus write

¹That is, we are isolating the contribution in the $p \rightarrow 0$ limit that is non-analytic in p . An essentially equivalent formulation is to define the SSC term as

$$T^{\text{SSC}}(\mathbf{k}_1, -\mathbf{k}_1, \mathbf{k}_2, -\mathbf{k}_2; \mathbf{p}) = \lim_{p \rightarrow 0} T_m(\mathbf{k}_1, -\mathbf{k}_1 + \mathbf{p}, \mathbf{k}_2, -\mathbf{k}_2 - \mathbf{p}) - T_m^{\text{cNG}}(\mathbf{k}_1, -\mathbf{k}_1, \mathbf{k}_2, -\mathbf{k}_2), \quad (3.8)$$

with the limit interpreted as keeping the leading term as $p \rightarrow 0$, which are terms $\propto P_L(p)$. This is also the formulation adopted in Sec. II. C of Ref. [17].

the SSC term as a single diagram:

$$\begin{aligned}
T^{\text{SSC}}(\mathbf{k}_1, -\mathbf{k}_1, \mathbf{k}_2, -\mathbf{k}_2; \mathbf{p}) &= \text{Diagram} \\
&= \mathcal{R}_1(k_1, -\mu_{\mathbf{p}, \mathbf{k}_1}) \mathcal{R}_1(k_2, \mu_{\mathbf{p}, \mathbf{k}_2}) P_m(k_1) P_m(k_2) P_L(p). \quad (3.10)
\end{aligned}$$

In this diagram, one of the vertices has incoming \mathbf{p} momentum while the other has $-\mathbf{p}$, hence the different signs on the second argument of the two \mathcal{R}_1 functions; numerically, this is however irrelevant because \mathcal{R}_1 is proportional to the square of this cosine angle (cf. Eq. (2.4)).

Returning to the calculation of the covariance, the non-Gaussian part in Eq. (3.6) can then be written as

$$\begin{aligned}
\text{Cov}^{\text{NG}}(k_1, k_2, \mu_{12}) &= \frac{1}{V_W} T_m^{\text{cNG}}(\mathbf{k}_1, -\mathbf{k}_1, \mathbf{k}_2, -\mathbf{k}_2) + \frac{1}{V_W^2} \int_{\mathbf{p}} |\tilde{W}(\mathbf{p})|^2 T_m^{\text{SSC}}(\mathbf{k}_1, -\mathbf{k}_1, \mathbf{k}_2, -\mathbf{k}_2; \mathbf{p}) \\
&= \text{Cov}^{\text{cNG}}(k_1, k_2, \mu_{12}) + \text{Cov}^{\text{SSC}}(k_1, k_2, \mu_{12}), \quad (3.11)
\end{aligned}$$

where the second line establishes our notation to denote the cNG and SSC matter covariance terms, and we have neglected the smoothing effect of the window function on the cNG term. Using Eqs. (2.4) and (3.10), the SSC term can be written explicitly as

$$\text{Cov}^{\text{SSC}}(k_1, k_2, \mu_{12}) = \text{Cov}_{\delta\delta}^{\text{SSC}} + \text{Cov}_{KK}^{\text{SSC}} + \text{Cov}_{\delta K}^{\text{SSC}} + \text{Cov}_{K\delta}^{\text{SSC}}, \quad (3.12)$$

with

$$V_W^2 \frac{\text{Cov}_{\delta\delta}^{\text{SSC}}(\mathbf{k}_1, \mathbf{k}_2)}{P_m(k_1) P_m(k_2)} = R_1(k_1) R_1(k_2) \int_{\mathbf{p}} |\tilde{W}(\mathbf{p})|^2 P_L(p) \quad (3.13)$$

$$V_W^2 \frac{\text{Cov}_{KK}^{\text{SSC}}(\mathbf{k}_1, \mathbf{k}_2)}{P_m(k_1) P_m(k_2)} = R_K(k_1) R_K(k_2) \int_{\mathbf{p}} |\tilde{W}(\mathbf{p})|^2 \left(\mu^2 - \frac{1}{3} \right) \left(\mu_{\mathbf{p}, \mathbf{k}_2}^2 - \frac{1}{3} \right) P_L(p) \quad (3.14)$$

$$V_W^2 \frac{\text{Cov}_{\delta K}^{\text{SSC}}(\mathbf{k}_1, \mathbf{k}_2)}{P_m(k_1) P_m(k_2)} = R_1(k_1) R_K(k_2) \int_{\mathbf{p}} |\tilde{W}(\mathbf{p})|^2 \left(\mu_{\mathbf{p}, \mathbf{k}_2}^2 - \frac{1}{3} \right) P_L(p) \quad (3.15)$$

$$V_W^2 \frac{\text{Cov}_{K\delta}^{\text{SSC}}(\mathbf{k}_1, \mathbf{k}_2)}{P_m(k_1) P_m(k_2)} = R_K(k_1) R_1(k_2) \int_{\mathbf{p}} |\tilde{W}(\mathbf{p})|^2 \left(\mu^2 - \frac{1}{3} \right) P_L(p), \quad (3.16)$$

where $\mu \equiv \mu_{\mathbf{p}, \mathbf{k}_1} = \mathbf{p} \mathbf{k}_1 / (p k_1)$ and $\mu_{\mathbf{p}, \mathbf{k}_2} = \mathbf{k}_2 \mathbf{p} / k_2 p = \sqrt{1 - \mu_{12}^2} \sqrt{1 - \mu^2} \cos \varphi + \mu \mu_{12}$.

The standard SSC term derived in Ref. [17] corresponds to the $\text{Cov}_{\delta\delta}^{\text{SSC}}$ part above, which describes the covariance due to the presence of a super-survey density perturbation. The other terms involve R_K and therefore correspond to the covariance that is induced by super-survey tidal fields. For the special case of isotropic window functions, $W(\mathbf{p}) = W(p)$, $\text{Cov}_{\delta K}^{\text{SSC}}$ and $\text{Cov}_{K\delta}^{\text{SSC}}$ vanish; the other term $\text{Cov}_{KK}^{\text{SSC}}$ also vanishes if one subsequently averages over μ_{12} . This reflects the physically expected result under spatial isotropy that the effect of tidal fields vanishes after averaging over all directions. We note however that all the terms in Eq. (3.12) are in general non-vanishing for the case of anisotropic window functions.

4 Lensing covariance

The expressions derived in the previous sections are for the three-dimensional matter power spectrum, which is not directly observable. Current and future large-scale structure surveys instead measure biased and redshift space distorted (RSD) versions of the matter density in the case of galaxy clustering, and a projected density field in the case of weak gravitational lensing. In this section, we focus on the latter; our derivation steps are analogous to those taken in the previous section.

4.1 Derivation

In General Relativity, the lensing convergence κ (see e.g. Refs. [44–47] for weak gravitational lensing reviews) can be given in terms of a weighted projection of the three dimensional density field as

$$\kappa(\boldsymbol{\theta}) = \int d\chi \, g(\chi) \, \delta(\mathbf{x} = \chi\boldsymbol{\theta}, z(\chi)), \quad (4.1)$$

where $\boldsymbol{\theta}$ is a two-dimensional position vector defined on the plane of the sky. Here, we have neglected higher-order corrections such as beyond-Born [48, 49], reduced-shear [50, 51] and lensing-bias contributions [52]. We have also assumed a spatially flat universe and replaced the two-dimensional Laplacian defined on the sky by the three-dimensional one to relate the lensing convergence to the three-dimensional density contrast using the Poisson equation; this is however a valid approximation in the small-scale, flat-sky limit that we assume in this paper. The variable $\chi \equiv \chi(z)$ is the comoving distance out to redshift z ($\chi = c \int_0^z dz' / (H(z'))$ in a spatially flat universe) and the function $g(\chi)$ is often called the lensing kernel or efficiency: for a single lensing source plane at χ_S it is given by $g(\chi, \chi_S) = (3H_0^2\Omega_m/2/c^2)(1+z)(\chi_S - \chi)\chi/\chi_S$.

Analogously to Eq. (3.1), we can define the observed convergence field as

$$\kappa_{\mathcal{W}}(\boldsymbol{\theta}) = \mathcal{W}(\boldsymbol{\theta})\kappa(\boldsymbol{\theta}), \quad (4.2)$$

where $\mathcal{W}(\boldsymbol{\theta})$ is now a window function defined on the sky that is unity within the surveyed area (solid angle $\Omega_{\mathcal{W}}$) and zero outside. Under the flat-sky approximation, the Fourier transform of the observed convergence reads (defining also a short-hand notation for two-dimensional volume integrals in Fourier space)

$$\tilde{\kappa}_{\mathcal{W}}(\boldsymbol{\ell}) = \int \frac{d^2\boldsymbol{\ell}'}{(2\pi)^2} \tilde{\mathcal{W}}(\boldsymbol{\ell}') \tilde{\kappa}(\boldsymbol{\ell} - \boldsymbol{\ell}') \equiv \int_{\boldsymbol{\ell}'} \tilde{\mathcal{W}}(\boldsymbol{\ell}') \tilde{\kappa}(\boldsymbol{\ell} - \boldsymbol{\ell}'), \quad (4.3)$$

with a power spectrum estimator that can be written as

$$\hat{C}(\boldsymbol{\ell}) = \frac{1}{\Omega_{\mathcal{W}}} \tilde{\kappa}_{\mathcal{W}}(\boldsymbol{\ell}) \tilde{\kappa}_{\mathcal{W}}(-\boldsymbol{\ell}). \quad (4.4)$$

Following the same reasoning as in after Eq. (3.4), this estimator is indeed an unbiased measure of the true power spectrum $C(\boldsymbol{\ell})$ defined as $(2\pi)^2 \delta_D(\boldsymbol{\ell} + \boldsymbol{\ell}') C(\boldsymbol{\ell}) = \langle \tilde{\kappa}(\boldsymbol{\ell}) \tilde{\kappa}(\boldsymbol{\ell}') \rangle$ for $\boldsymbol{\ell} \gg 2\pi/\theta_0$, where $\theta_0 \sim \Omega_{\mathcal{W}}^{1/2}$ is the typical survey window size.

The sample covariance can then be written as

$$\begin{aligned}
\text{Cov}_\kappa(\ell_1, \ell_2) &= \langle \hat{C}(\ell_1) \hat{C}(\ell_2) \rangle - \langle \hat{C}(\ell_1) \rangle \langle \hat{C}(\ell_2) \rangle \\
&= \frac{1}{\Omega_{\mathcal{W}}^2} \left[\langle \tilde{\kappa}_{\mathcal{W}}(\ell_1) \tilde{\kappa}_{\mathcal{W}}(\ell_2) \rangle \tilde{\kappa}_{\mathcal{W}}(-\ell_1) \tilde{\kappa}_{\mathcal{W}}(-\ell_2) \rangle + (\ell_2 \leftrightarrow -\ell_2) \right] \\
&\quad + \frac{1}{\Omega_{\mathcal{W}}^2} \langle \tilde{\kappa}_{\mathcal{W}}(\ell_1) \tilde{\kappa}_{\mathcal{W}}(-\ell_1) \tilde{\kappa}_{\mathcal{W}}(\ell_2) \tilde{\kappa}_{\mathcal{W}}(-\ell_2) \rangle_c.
\end{aligned} \tag{4.5}$$

Following similar steps as for the three-dimensional case, we straightforwardly arrive at

$$\begin{aligned}
\text{Cov}_\kappa(\ell_1, \ell_2) &= \frac{1}{\Omega_{\mathcal{W}}^2} [C(\ell_1)]^2 \left[|\tilde{\mathcal{W}}(\ell_1 + \ell_2)|^2 + |\tilde{\mathcal{W}}(\ell_1 - \ell_2)|^2 \right] \\
&\quad + \frac{1}{\Omega_{\mathcal{W}}^2} \int_{\ell} |\tilde{\mathcal{W}}(\ell)|^2 \mathcal{T}_\kappa(\ell_1, -\ell_1 + \ell, \ell_2, -\ell_2 - \ell),
\end{aligned} \tag{4.6}$$

with $(2\pi)^2 \delta_D(\ell_{abcd}) \mathcal{T}_\kappa(\ell_a, \ell_b, \ell_c, \ell_d) = \langle \tilde{\kappa}(\ell_a) \tilde{\kappa}(\ell_b) \tilde{\kappa}(\ell_c) \tilde{\kappa}(\ell_d) \rangle_c$ defining the trispectrum of the convergence field. We refer to the first and second terms on the right-hand side as the Gaussian, $\text{Cov}_\kappa^{\text{G}}$, and non-Gaussian contributions to the convergence covariance, respectively. Under the Limber approximation (we discuss its implementation in Appendix C), the convergence power spectrum and trispectrum can be related to those of the three-dimensional density contrast as²

$$C(\ell) = \int d\chi [g(\chi)]^2 \chi^{-2} P_m \left(\mathbf{k} = \frac{\ell}{\chi}; z(\chi) \right) \tag{4.7}$$

$$\mathcal{T}_\kappa(\ell_a, \ell_b, \ell_c, \ell_d) = \int d\chi [g(\chi)]^4 \chi^{-6} T_m \left(\frac{\ell_a}{\chi}, \frac{\ell_b}{\chi}, \frac{\ell_c}{\chi}, \frac{\ell_d}{\chi}; z(\chi) \right). \tag{4.8}$$

Using the split of the matter trispectrum into its degenerate and super-sample parts, the Gaussian, cNG and SSC contributions to the lensing convergence covariance can be given, respectively, as

$$\text{Cov}_\kappa^{\text{G}}(\ell_1, \ell_2) = \frac{1}{\Omega_{\mathcal{W}}^2} [C(\ell_1)]^2 \left[|\tilde{\mathcal{W}}(\ell_1 + \ell_2)|^2 + |\tilde{\mathcal{W}}(\ell_1 - \ell_2)|^2 \right] \tag{4.9}$$

$$\text{Cov}_\kappa^{\text{cNG}}(\ell_1, \ell_2) = \frac{1}{\Omega_{\mathcal{W}}^2} \int d\chi [g(\chi)]^4 \chi^{-6} T_m^{\text{cNG}} \left(\frac{\ell_1}{\chi}, -\frac{\ell_1}{\chi}, \frac{\ell_2}{\chi}, -\frac{\ell_2}{\chi}; z(\chi) \right) \tag{4.10}$$

$$\begin{aligned}
\text{Cov}_\kappa^{\text{SSC}}(\ell_1, \ell_2) &= \frac{1}{\Omega_{\mathcal{W}}^2} \int d\chi [g(\chi)]^4 \chi^{-6} \int_{\ell} |\tilde{\mathcal{W}}(\ell)|^2 T^{\text{SSC}} \left(\frac{\ell_1}{\chi}, -\frac{\ell_1}{\chi}, \frac{\ell_2}{\chi}, -\frac{\ell_2}{\chi}; \frac{\ell}{\chi} \right) \\
&= \text{Cov}_{\kappa\delta\delta}^{\text{SSC}} + \text{Cov}_{\kappa KK}^{\text{SSC}} + \text{Cov}_{\kappa\delta K}^{\text{SSC}} + \text{Cov}_{\kappa K\delta}^{\text{SSC}}.
\end{aligned} \tag{4.11}$$

²These expressions become more accurate with the replacement $\ell_n/\chi \rightarrow \sqrt{\ell_n(\ell_n + 1)} \hat{\ell}_n/\chi$ in the arguments of the power spectrum and trispectrum. For notational simplicity, however, we simply write ℓ_n/χ .

In Eq. (4.11), we have again split the SSC contribution into four pieces given by

$$\begin{aligned} \text{Cov}_{\kappa\delta\delta}^{\text{SSC}}(\ell_1, \ell_2) &= \frac{1}{\Omega_{\mathcal{W}}^2} \int d\chi [g(\chi)]^4 \chi^{-6} R_1\left(\frac{l_1}{\chi}, \chi\right) R_1\left(\frac{l_2}{\chi}, \chi\right) P_m\left(\frac{l_1}{\chi}, \chi\right) P_m\left(\frac{l_2}{\chi}, \chi\right) \\ &\quad \times \int_{\ell} |\tilde{\mathcal{W}}(\ell)|^2 P_L\left(\frac{\ell}{\chi}, \chi\right), \end{aligned} \quad (4.12)$$

$$\begin{aligned} \text{Cov}_{\kappa KK}^{\text{SSC}}(\ell_1, \ell_2) &= \frac{1}{\Omega_{\mathcal{W}}^2} \int d\chi [g(\chi)]^4 \chi^{-6} R_K\left(\frac{l_1}{\chi}, \chi\right) R_K\left(\frac{l_2}{\chi}, \chi\right) P_m\left(\frac{l_1}{\chi}, \chi\right) P_m\left(\frac{l_2}{\chi}, \chi\right) \\ &\quad \times \int_{\ell} |\tilde{\mathcal{W}}(\ell)|^2 \left(\mu^2 - \frac{1}{3}\right) \left(\mu_{\ell, \ell_2}^2 - \frac{1}{3}\right) P_L\left(\frac{\ell}{\chi}, \chi\right), \end{aligned} \quad (4.13)$$

$$\begin{aligned} \text{Cov}_{\kappa\delta K}^{\text{SSC}}(\ell_1, \ell_2) &= \frac{1}{\Omega_{\mathcal{W}}^2} \int d\chi [g(\chi)]^4 \chi^{-6} R_1\left(\frac{l_1}{\chi}, \chi\right) R_K\left(\frac{l_2}{\chi}, \chi\right) P_m\left(\frac{l_1}{\chi}, \chi\right) P_m\left(\frac{l_2}{\chi}, \chi\right) \\ &\quad \times \int_{\ell} |\tilde{\mathcal{W}}(\ell)|^2 \left(\mu_{\ell, \ell_2}^2 - \frac{1}{3}\right) P_L\left(\frac{\ell}{\chi}, \chi\right), \end{aligned} \quad (4.14)$$

$$\begin{aligned} \text{Cov}_{\kappa K\delta}^{\text{SSC}}(\ell_1, \ell_2) &= \frac{1}{\Omega_{\mathcal{W}}^2} \int d\chi [g(\chi)]^4 \chi^{-6} R_K\left(\frac{l_1}{\chi}, \chi\right) R_1\left(\frac{l_2}{\chi}, \chi\right) P_m\left(\frac{l_1}{\chi}, \chi\right) P_m\left(\frac{l_2}{\chi}, \chi\right) \\ &\quad \times \int_{\ell} |\tilde{\mathcal{W}}(\ell)|^2 \left(\mu^2 - \frac{1}{3}\right) P_L\left(\frac{\ell}{\chi}, \chi\right), \end{aligned} \quad (4.15)$$

where $\mu = \ell\ell_1/\ell\ell_1$ and $\mu_{\ell\ell_2} = \ell\ell_2/\ell\ell_2$.

An interesting take-away message from the above equations is that, contrary to the three-dimensional case, all terms are in general non-vanishing, even for isotropic survey window functions on the sky. This is because the projection onto the sky, i.e. integration along the line of sight, that is performed to obtain lensing observables effectively breaks statistical isotropy, and leads to a coupling to super-survey tidal fields.³ As a result, the integrals over the window function (which are now two-dimensional) do not vanish for any of the four SSC contributions, even for $\tilde{\mathcal{W}}(\ell) = \tilde{\mathcal{W}}(\ell)$, as they do in the three-dimensional case. Further, the additional SSC terms are in general non-negligible. For instance, denoting by $\sigma_{\mathcal{W},\delta\delta}^2$ the factor in the second line of Eq. (4.12), and further assuming an isotropic survey window function, $\tilde{\mathcal{W}}(\ell) = \tilde{\mathcal{W}}(\ell)$, the same corresponding integrals in the remaining SSC terms are given by $\sigma_{\mathcal{W},\delta K}^2 = \sigma_{\mathcal{W},K\delta}^2 = \sigma_{\mathcal{W},\delta\delta}^2/6$ and $\sigma_{\mathcal{W},KK}^2 = \sigma_{\mathcal{W},\delta\delta}^2[2 - 9\cos(2\theta_{12})]/72$, with θ_{12} defined as $\cos(\theta_{12}) = \mu_{\ell_1\ell_2} = \ell_1\ell_2/\ell_1/\ell_2$. Further averaging as $\int_0^\pi d\theta_{12}/\pi$ we get $\sigma_{\mathcal{W},KK}^2 = \sigma_{\mathcal{W},\delta\delta}^2/36$. Next, we quantitatively investigate the size of these terms for an idealized lensing survey.

4.2 Numerical results

In order to display the results from the above equations, we adopt a Λ CDM cosmology with parameters $\Omega_m h^2 = 0.1249$, $\Omega_b h^2 = 0.02205$, $h = 0.70$, $n_s = 0.96$, $\sigma_8(z=0) = 0.83$. We evaluate linear and nonlinear three-dimensional matter power spectra using CLASS [53] with the HALOFIT prescription of Ref. [54]. We consider a survey with area $\Omega_{\mathcal{W}} = f_{\text{sky}} 4\pi \approx 15000 \text{ deg}^2$ ($f_{\text{sky}} \approx 0.36$), and a single source redshift of $z_S = 1$. We also limit ourselves to showing only the monopole part of the lensing covariance, i.e., that which is obtained after averaging over θ_{12} . This corresponds to the covariance of the angle-averaged power spectrum

³This is analogous to the recent discussion in Refs. [41, 42] in which RSD effects also break statistical isotropy and therefore are also susceptible to be affected by super-survey tidal fields, even in the case of isotropic window functions.

estimator

$$\hat{C}(\ell_1) = \frac{1}{\Omega_{\mathcal{W}}} \int_{\Omega_{\ell_1}} \frac{d^2\ell}{2\pi\ell_1\Delta_{\ell_1}} \tilde{\kappa}_{\mathcal{W}}(\ell) \tilde{\kappa}_{\mathcal{W}}(-\ell), \quad (4.16)$$

where the integral is taken over an annulus of width Δ_{ℓ_1} centered at ℓ_1 . We also take into account the contribution from shot noise in shape measurements, which is given by $C^{\text{noise}} = \sigma_e^2/(2\bar{n}_{\text{gal}})$; we consider $\bar{n}_{\text{gal}} = 30 \text{ arcmin}^{-2}$ and $\sigma_e = 0.37$ (defined per galaxy).

We thus evaluate the angle-averaged Gaussian covariance as

$$\text{Cov}_{\kappa}^G(\ell_i, \ell_j) = \frac{4\pi}{\Omega_{\mathcal{W}}\ell_i\Delta_{\ell,i}} \left[C(\ell_i) + \frac{\sigma_e^2}{2\bar{n}_{\text{gal}}} \right]^2 \delta_{ij}, \quad (4.17)$$

where $\Delta_{\ell,i}$ is the width of the bin labeled by i and the Kronecker delta δ_{ij} ensures that the Gaussian term contributes only to the diagonal of the covariance matrix. We take ℓ bins equally spaced in log-scale with $\Delta \log \ell = 0.12$. We evaluate the cNG contribution using Eq. (4.10), with the response-based calculation of the angle-averaged T_m^{cNG} presented in Ref. [16]. For the SSC term, we use the equations derived above (cf. Eqs. (4.11)-(4.15)) for a disk-shaped survey geometry with radius $\theta_{\mathcal{W}} = \sqrt{\Omega_{\mathcal{W}}/\pi}$ as window function

$$\mathcal{W}(\boldsymbol{\theta}) \equiv \mathcal{W}(\theta) = \begin{cases} 1 & , \text{ if } \theta \leq \theta_{\mathcal{W}} \\ 0 & , \text{ otherwise,} \end{cases} \quad (4.18)$$

for which

$$|\tilde{\mathcal{W}}(\boldsymbol{\ell})|^2 \equiv |\tilde{\mathcal{W}}(\ell)|^2 = \Omega_{\mathcal{W}}^2 \left[\frac{2J_1(\ell\theta_{\mathcal{W}})}{\ell\theta_{\mathcal{W}}} \right]^2, \quad (4.19)$$

where $J_1(x)$ is the first order Bessel function of first kind. Naturally, our assumption of a disk-like window function may not be representative of the general anisotropic and irregular masks that characterize real surveys. We choose to adopt this geometry for simplicity of calculation and because it is sufficient for the purpose of estimating the size of the anisotropic contributions in the SSC term. We leave the exploration of more general window functions for future work. Note that asymmetric window functions will in general act to increase the tidal SSC contributions.

The color maps in Fig. 2 show the SSC (left), and the sum of the Gaussian and connected non-Gaussian (right) contributions to the total covariance of the lensing convergence power spectrum. Figure 3 shows a few *slices* of the various contributions at constant ℓ_2 , as labeled. The two left panels of Fig. 4 show the same, but along the diagonal $\ell_1 = \ell_2$. Finally, the two right panels of Fig. 4 show the signal-to-noise ratio defined as

$$\left(\frac{S}{N} \right)^2 = \sum_{\ell_1, \ell_2 < \ell_{\text{max}}} C(\ell_1) \text{Cov}^{-1}(\ell_1, \ell_2) C(\ell_2), \quad (4.20)$$

as a function of the maximum wavenumber ℓ_{max} . This helps to quantify the loss of information caused by the various contributions to the covariance matrix.

Figures 2, 3 and 4 illustrate the following main points:

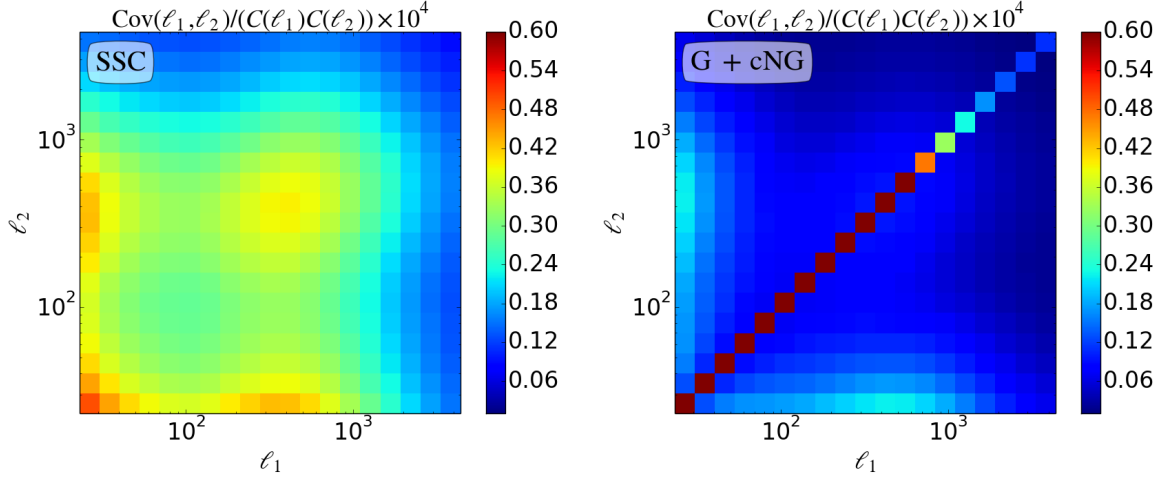


Figure 2. Contributions to the angle-averaged lensing convergence covariance matrix. The left color map shows the SSC covariance contribution computed with Eq. (4.11) for a disk-like survey geometry (cf. Eq. (4.19)). The right color map shows the same, but for the sum of the Gaussian (cf. Eq. (4.17)) and connected non-Gaussian contributions (cf. Eq. (4.10) with the response-based calculation of Ref. [16]). In the right panel, the diagonal terms up to $\ell_1, \ell_2 \sim 500$ are higher than the maximum of the color scale (i.e., the color scale saturates) to facilitate visualization of the off-diagonal terms.

1. The SSC is the dominant off-diagonal contribution. For Euclid- and LSST-like surveys, which will observe about 30 – 40% of the sky, these results suggest that the SSC contribution constitutes a significant portion of the statistical error that cannot be ignored.
2. The summed contribution from the tidal SSC terms derived in this paper (cf. Eqs. (4.13), (4.14), (4.15); dashed green lines labeled with SSC_{tidal}) are smaller than the purely isotropic term derived in Ref. [17] (cf. Eq. (4.12)), but are still sizable contributions to the covariance. For instance, on the diagonal (cf. left panels of Fig. 4), these terms constitute $\approx 15\%$ of the total covariance matrix at $\ell \approx 1000$. In fact, for our simple survey setup, these new SSC terms are comparable to the cNG covariance contribution; they also induce similar degradations in signal-to-noise, compared to the purely Gaussian case (cf. orange lines in Fig. 4).
3. The degradation in signal-to-noise caused by the new SSC terms and the cNG terms compared to a case with Gaussian and purely isotropic SSC (labeled as $SSC_{\delta\delta}$) is however small (cf. red vs. magenta lines in the right panels of Fig. 4). This means that the loss in signal-to-noise compared to a Gaussian only case is still largely dominated by the $\text{Cov}_{\kappa\delta\delta}^{SSC}$ term.

The conclusions drawn above should be interpreted in light of the rather simplistic survey setup adopted. The exact relative contribution of the various terms can depend sensitively on the shape of the source galaxy redshift distribution and number of tomographic bins used, as well as on the shape of the window function for the case of the SSC terms. In particular, our results here correspond to an isotropic survey window function, but it is reasonable to expect that more realistic anisotropic masks may increase the size of the tidal

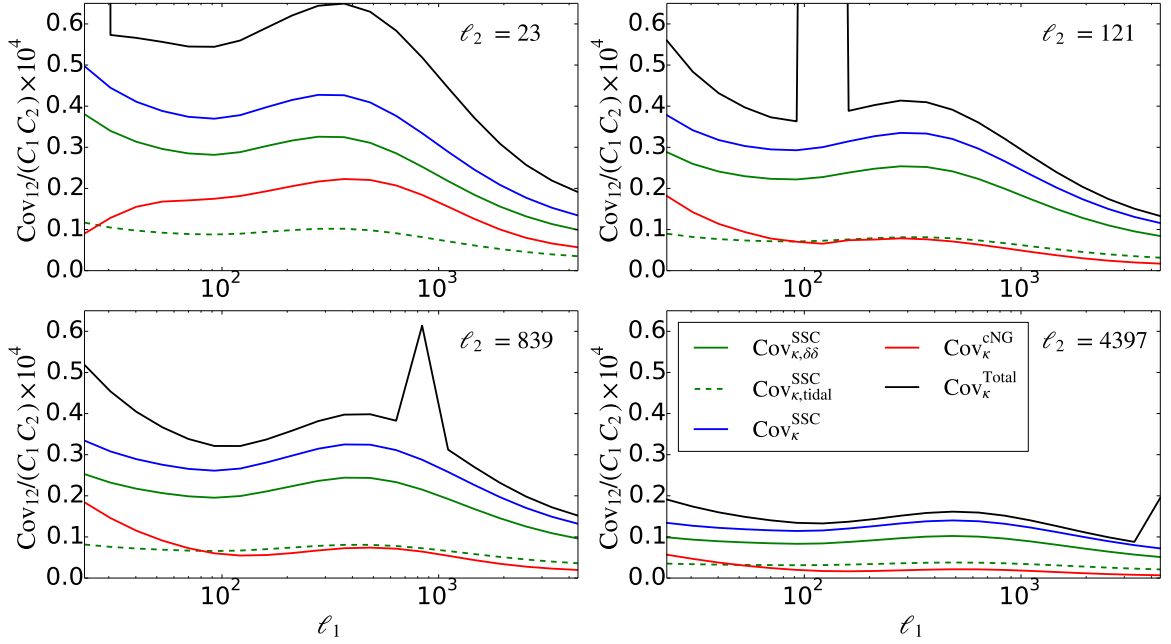


Figure 3. Angle-averaged lensing convergence covariance matrix as a function of ℓ_1 , for fixed values of ℓ_2 , as labeled. The solid and dashed green lines show the contributions to the total SSC term of Eq. (4.12) and summed Eqs. (4.13)-(4.15), respectively; the blue line shows the full SSC. The red line shows the connected non-Gaussian term computed using Eq. (4.10) with the response calculation of Ref. [16]. The black solid line shows the total lensing covariance, including the Gaussian contribution. In the labels, $\text{Cov}_{12} = \text{Cov}(\ell_1, \ell_2)$ and $C_i = C(\ell_i)$.

SSC terms derived here (see e.g. Ref. [22] for a study on the impact of the shape of the window function on the isotropic SSC term; Ref. [55] also evaluates the isotropic SSC term for an anisotropic footprint). We leave these developments for a future dedicated forecast study where we will aim to quantify the importance of the various covariance contributions for current (e.g. KiDS [6] and DES [9, 10]) and future surveys.

Another caveat is that we have relied on a physically motivated, but heuristic guess for the tidal response coefficient $R_K(k)$ (Eq. (2.5)). However, given that the shape of the different isotropic growth-only response coefficients $G_n(k)$ were found to be quite similar [26], which is what we assumed for $R_K(k)$, and given the very good agreement of the response prediction including R_K with the cNG covariance measured in simulations [16], we expect the actual $R_K(k)$ to not differ significantly from the estimate used here; this should nonetheless be quantitatively checked once separate universe measurements of $R_K(k)$ become available.

5 Summary and conclusions

We have used the response-based extension of perturbation theory to derive the full super-sample contribution to the covariance of the matter as well as lensing convergence power spectrum. The original derivation of Ref. [17] described the contribution given by the response of the power spectrum to purely isotropic super-survey modes (cf. $\delta\delta$ term in Eqs. (3.12) and (4.11)). Here, we have derived the remainder of the lensing SSC, which corresponds to terms that involve the response of the power spectrum to super-survey tidal-fields (cf. KK , δK , $K\delta$

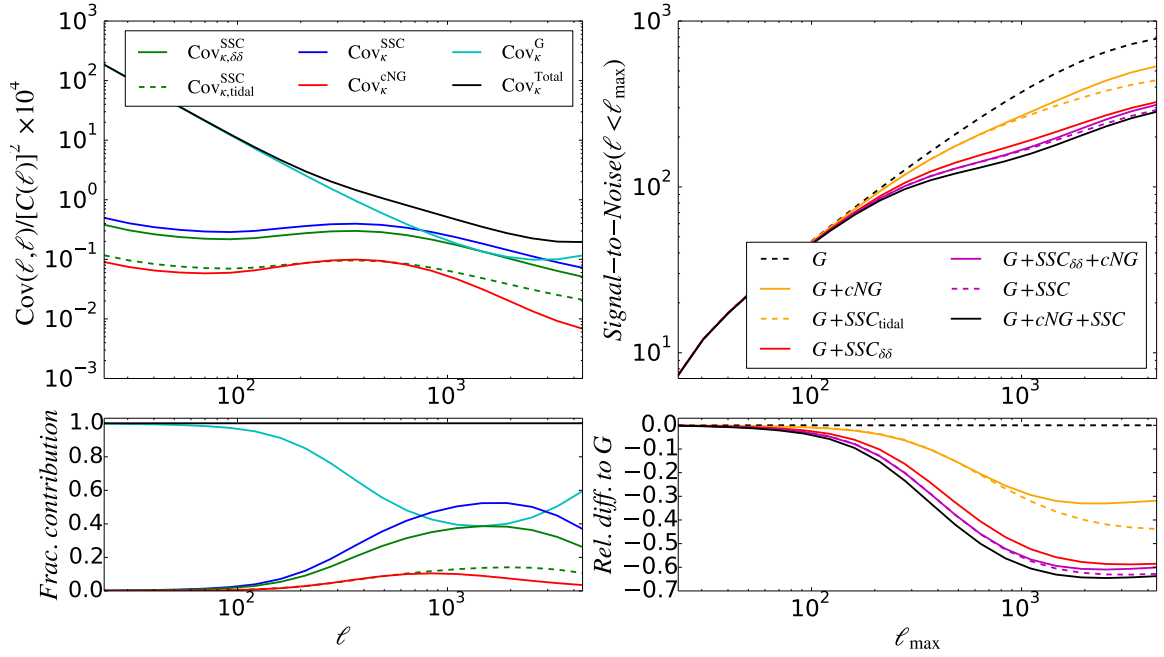


Figure 4. The upper left panel shows the same as Fig. 3, but along the diagonal of the covariance matrix, $\ell_1 = \ell_2$; the lower left panel shows the fractional size of each contribution to the total covariance. The upper right panel shows the signal-to-noise ratio as a function of ℓ_{max} (cf. Eq. 4.20); the lower right panel shows the relative difference to the Gaussian-only case.

terms in Eqs. (3.12) and (4.11)). Our response-based derivation proved particularly useful in clarifying the origin of all the terms that make up the SSC contribution.

By adopting an idealized lensing survey setup for a surveyed sky fraction of $f_{\text{sky}} \approx 0.36$, single source redshift at $z_S = 1$ and isotropic window function, we have demonstrated that the contribution from the tidal SSC terms derived here can be sizable, contributing up to 20 – 25% of the total SSC term. This number should be taken under the caveat that we have used a physical guess for the growth part of the tidal response coefficient $R_K(k)$. Given that the SSC term can provide the dominant off-diagonal contribution to the lensing covariance matrix, it is therefore recommendable that these additional terms be included in future parameter inference analyses using weak lensing data.

The results presented here correspond to the case of an isotropic survey window function (cf. Eq. (4.18)). In general, real surveys will have anisotropic window functions, which could further enhance the relative contribution of the tidal SSC terms derived here. The exploration of the dependence of the relative importance of the various SSC components on the shape of the window function, as well as more realistic source redshift distribution functions (including tomography) will appear in a follow-up forecast study.

The cosmological analysis of large-scale structure surveys is naturally not limited to lensing observations. In recent works within the KiDS [7, 8] and DES [10] collaborations, the resulting parameter constraints were obtained from a joint analysis of lensing and projected galaxy two-point statistics, including their cross-correlation. Future observational efforts are likely to involve similar such combined analyses. The response formalism can also in principle be extended to galaxies as density tracers and be used to calculate the corresponding cNG and SSC terms of their auto power spectrum, as well as of the cross-spectrum with

lensing. This will require separate universe measurements of the responses of the galaxy power spectrum (see e.g. Ref. [42] for a measurement of such response coefficients using power spectra measured in sub-volumes of a periodic N -body simulation box).

Finally, we note that the steps that we have taken here can be applied also to the calculation of the super-sample bispectrum covariance. The inclusion of the bispectrum in cosmological analyses can improve parameter constraints [34, 37, 56], and as a result, it is important that its covariance matrix (and cross-covariance with the power spectrum) is equally well understood. In Ref. [57], the authors have taken the first steps in this direction, but similarly to Ref. [17], their results take into account only responses to isotropic super-survey modes computed using the halo model. Within the response formalism, the generalization to the case of the bispectrum is straightforward, but will require simulation measurements of the first order bispectrum response coefficients, which can be done with the separate universe technique.

Acknowledgments

We thank Kazuyuki Akitsu, Fabien Lacasa, Yin Li, Takahiro Nishimichi, and Masahiro Takada for useful comments and discussions. FS acknowledges support from the Starting Grant (ERC-2015-STG 678652) “GrInflaGal” from the European Research Council. EK acknowledges support from NASA grant 15-WFIRST15-0008 Cosmology with the High Latitude Survey WFIRST Science Investigation Team (SIT).

A Derivation of the three-dimensional matter covariance with a finite window

In this appendix, we show a few of the intermediate steps taken when deriving Eq. (3.6) from Eq. (3.5). The following is an identity that will be useful below:

$$\tilde{W}(\mathbf{k}) = \int_{\mathbf{p}} \tilde{W}(\mathbf{p}) \tilde{W}(\mathbf{k} - \mathbf{p}) = \left[\prod_{i=1}^n \int_{\mathbf{p}_i} \tilde{W}(\mathbf{p}_i) \right] (2\pi)^3 \delta_D(\mathbf{k} - \mathbf{p}_{12..n}), \quad (\text{A.1})$$

which follows from the fact that the window function we defined in real space satisfies $W^n(\mathbf{x}) = W(\mathbf{x})$.

Rewriting Eq. (3.5) here, we have

$$\begin{aligned} \text{Cov}(\mathbf{k}_1, \mathbf{k}_2) &= \langle \hat{P}_W(\mathbf{k}_1) \hat{P}_W(\mathbf{k}_2) \rangle - \langle \hat{P}_W(\mathbf{k}_1) \rangle \langle \hat{P}_W(\mathbf{k}_2) \rangle \\ &= \frac{1}{V_W^2} \left[\langle \tilde{\delta}_W(\mathbf{k}_1) \tilde{\delta}_W(\mathbf{k}_2) \rangle \langle \tilde{\delta}_W(-\mathbf{k}_1) \tilde{\delta}_W(-\mathbf{k}_2) \rangle + (\mathbf{k}_2 \leftrightarrow -\mathbf{k}_2) \right] \\ &\quad + \frac{1}{V_W^2} \langle \tilde{\delta}_W(\mathbf{k}_1) \tilde{\delta}_W(-\mathbf{k}_1) \tilde{\delta}_W(\mathbf{k}_2) \tilde{\delta}_W(-\mathbf{k}_2) \rangle_c. \end{aligned} \quad (\text{A.2})$$

The terms inside square brackets in Eq. (A.2) can be worked out as

$$\begin{aligned}
& \langle \tilde{\delta}_W(\mathbf{k}_1) \tilde{\delta}_W(\mathbf{k}_2) \rangle \langle \tilde{\delta}_W(-\mathbf{k}_1) \tilde{\delta}_W(-\mathbf{k}_2) \rangle = \\
& = \left[\prod_{i=1}^4 \int_{\mathbf{p}_i} \tilde{W}(\mathbf{p}_i) \right] (2\pi)^3 \delta_D(\mathbf{k}_{12} - \mathbf{p}_{12}) (2\pi)^3 \delta_D(-\mathbf{k}_{12} - \mathbf{p}_{34}) P_m(\mathbf{k}_1 - \mathbf{p}_1) P_m(\mathbf{k}_1 + \mathbf{p}_3) \\
& = [P_m(\mathbf{k}_1)]^2 \int_{\mathbf{p}_1} \int_{\mathbf{p}_2} \int_{\mathbf{p}_3} \tilde{W}(\mathbf{p}_1) \tilde{W}(\mathbf{p}_2) \tilde{W}(\mathbf{p}_3) \tilde{W}(-\mathbf{k}_{12} - \mathbf{p}_3) (2\pi)^3 \delta_D(\mathbf{k}_{12} - \mathbf{p}_{12}) \\
& = [P_m(\mathbf{k}_1)]^2 \int_{\mathbf{p}_3} \tilde{W}(\mathbf{k}_{12}) \tilde{W}(\mathbf{p}_3) \tilde{W}(-\mathbf{k}_{12} - \mathbf{p}_3) \\
& = [P_m(\mathbf{k}_1)]^2 |\tilde{W}(\mathbf{k}_{12})|^2. \tag{A.3}
\end{aligned}$$

In the first equality above, we used Eq. (3.2) and the definition of the power spectrum; in the second equality, the integral over \mathbf{p}_4 eliminates one Dirac-delta and the approximation $P_m(\mathbf{k}_1 + \mathbf{p}_i) \approx P_m(\mathbf{k}_1)$ allows us to move the power spectra terms out of the integrals; in the third equality we used Eq. (A.1) for $n = 2$, and then again in the fourth equality. This result is that of the first term on the right-hand side of Eq. (3.6).

The derivation of the connected four-point function term in Eq. (A.2) can be done as follows

$$\begin{aligned}
& \langle \tilde{\delta}_W(\mathbf{k}_1) \tilde{\delta}_W(-\mathbf{k}_1) \tilde{\delta}_W(\mathbf{k}_2) \tilde{\delta}_W(-\mathbf{k}_2) \rangle_c = \\
& = \left[\prod_{i=1}^4 \int_{\mathbf{p}_i} \tilde{W}(\mathbf{p}_i) \right] (2\pi)^3 \delta_D(\mathbf{p}_{1234}) T_m(\mathbf{k}_1 - \mathbf{p}_1, -\mathbf{k}_1 - \mathbf{p}_2, \mathbf{k}_2 - \mathbf{p}_3, -\mathbf{k}_2 - \mathbf{p}_4) \\
& = \left[\prod_{i=1}^4 \int_{\mathbf{p}_i} \tilde{W}(\mathbf{p}_i) \right] (2\pi)^3 \delta_D(\mathbf{p}_{1234}) T_m(\mathbf{k}_1, -\mathbf{k}_1 - \mathbf{p}_{12}, \mathbf{k}_2, -\mathbf{k}_2 - \mathbf{p}_{34}) \\
& = \int_{\mathbf{p}_1} \int_{\mathbf{p}_2} \int_{\mathbf{p}_3} \tilde{W}(\mathbf{p}_1) \tilde{W}(\mathbf{p}_2) \tilde{W}(\mathbf{p}_3) \tilde{W}(-\mathbf{p}_{123}) T_m(\mathbf{k}_1, -\mathbf{k}_1 - \mathbf{p}_{12}, \mathbf{k}_2, -\mathbf{k}_2 + \mathbf{p}_{12}). \tag{A.4}
\end{aligned}$$

The first equality again simply uses the definition of the matter trispectrum and of the observed density contrast Eq. (3.2). In the second equality, we have performed the change of variables $\mathbf{k}_1 - \mathbf{p}_1 \rightarrow \mathbf{k}_1$, $\mathbf{k}_2 - \mathbf{p}_3 \rightarrow \mathbf{k}_2$, which is allowed under the assumed limit that $k_i \gg p_i$; in the third equality, we have integrated over \mathbf{p}_4 . From hereon, the steps involve manipulations of the integrals over the window functions. Defining a new integration variable $\mathbf{p} = \mathbf{p}_{12}$, Eq. (A.4) continues as

$$\begin{aligned}
& \int_{\mathbf{p}_1} \int_{\mathbf{p}} \int_{\mathbf{p}_3} \tilde{W}(\mathbf{p}_1) \tilde{W}(\mathbf{p} - \mathbf{p}_1) \tilde{W}(\mathbf{p}_3) \tilde{W}(-\mathbf{p} - \mathbf{p}_3) T_m(\mathbf{k}_1, -\mathbf{k}_1 - \mathbf{p}, \mathbf{k}_2, -\mathbf{k}_2 + \mathbf{p}) \\
& = \int_{\mathbf{p}} |W(\mathbf{p})|^2 T_m(\mathbf{k}_1, -\mathbf{k}_1 + \mathbf{p}, \mathbf{k}_2, -\mathbf{k}_2 - \mathbf{p}), \tag{A.5}
\end{aligned}$$

where we have used Eq. (A.1) for $n = 1$ twice in the integrals over \mathbf{p}_1 and \mathbf{p}_3 . This matches the result of Eq. (3.6).

B The super sample term at tree level

To build intuition about the origin of the super-sample term derived in Sec. 3.2, it is instructive to understand how it arises at tree level in perturbation theory (see also Appendix A of

Ref. [12]). The tree-level matter trispectrum is given by

$$T_m(\mathbf{k}_a, \mathbf{k}_b, \mathbf{k}_c, \mathbf{k}_d) = \left[6F_3(\mathbf{k}_a, \mathbf{k}_b, \mathbf{k}_c)P_L(k_a)P_L(k_b)P_L(k_c) + 3 \text{ perm.} \right] \\ + \left[4F_2(-\mathbf{k}_{ab}, \mathbf{k}_b)F_2(\mathbf{k}_{ab}, \mathbf{k}_c)P_L(|\mathbf{k}_{ab}|)P_L(k_b)P_L(k_c) + 11 \text{ perm.} \right], \quad (\text{B.1})$$

where F_2 and F_3 are the second- and third-order perturbation theory kernels. By specializing to the relevant configuration, it is straightforward to show that (always implicitly assuming $p \ll k_1, k_2$)

$$T_m(\mathbf{k}_1, -\mathbf{k}_1 + \mathbf{p}, \mathbf{k}_2, -\mathbf{k}_2 - \mathbf{p}) \approx \underbrace{T_m^{\text{cNG, tree}}(\mathbf{k}_1, -\mathbf{k}_1, \mathbf{k}_2, -\mathbf{k}_2)}_{4F_3 \text{ terms} + 8F_2^2 \text{ terms}} + \underbrace{T_m^{\text{SSC, tree}}(\mathbf{k}_1, -\mathbf{k}_1, \mathbf{k}_2, -\mathbf{k}_2; \mathbf{p})}_{4F_2^2 \text{ terms}}. \quad (\text{B.2})$$

That is, out of the 16 permutations in Eq. (B.1), there are 12 that asymptote to a finite value as $p \rightarrow 0$. These correspond to the standard connected non-Gaussian tree-level covariance (see e.g. Eq. (3.1) of Ref. [16]). The remaining four permutations of Eq. (B.1) are $\propto P_L(p)$, and are thus precisely the terms isolated by the limit in Eq. (3.9). These therefore represent the SSC term. Diagrammatically, at tree level we have

$$T^{\text{SSC, tree}}(\mathbf{k}_1, -\mathbf{k}_1, \mathbf{k}_2, -\mathbf{k}_2; \mathbf{p}) = \left[\begin{array}{c} \text{Diagram: } \mathbf{k}_1 \text{ and } -\mathbf{k}_1 + \mathbf{p} \text{ enter a vertex } F_2, \text{ which connects to a vertex } F_2 \text{ via } P_L(p). \text{ From this second vertex, } \mathbf{k}_2 \text{ and } -\mathbf{k}_2 - \mathbf{p} \text{ exit.} \\ + (\mathbf{k}_1 \leftrightarrow -\mathbf{k}_1 + \mathbf{p}) \\ + (\mathbf{k}_2 \leftrightarrow -\mathbf{k}_2 - \mathbf{p}) \end{array} \right] \\ = \left[2F_2(\mathbf{k}_1 - \mathbf{p}, \mathbf{p})P_L(|\mathbf{k}_1 - \mathbf{p}|) + 2F_2(\mathbf{k}_1, -\mathbf{p})P_L(k_1) \right] \\ \times \left[2F_2(\mathbf{k}_2 + \mathbf{p}, -\mathbf{p})P_L(|\mathbf{k}_2 + \mathbf{p}|) + 2F_2(\mathbf{k}_2, \mathbf{p})P_L(k_2) \right] P_L(p) \\ = \mathcal{R}_1^{\text{tree}}(k_1, -\mu_{\mathbf{p}, \mathbf{k}_1})\mathcal{R}_1^{\text{tree}}(k_2, \mu_{\mathbf{p}, \mathbf{k}_2})P_L(k_1)P_L(k_2)P_L(p), \quad (\text{B.3})$$

where in the last equality we have used the tree level limit of the first order response \mathcal{R}_1 derived in Ref. [15]. The expression above is only valid if all modes are in the linear regime $k_1, k_2, p \ll k_{\text{NL}}$. However, the resummed response vertices, obtained using simulation measurements [18, 26] of the first order response R_1, R_K (cf. Fig. 1), allow us to be predictive for $p \ll k_{\text{NL}}$, but any nonlinear k_1, k_2 .

C The Limber approximation in the convergence trispectrum

The Limber approximation dramatically simplifies the calculation of weak lensing statistics, in particular of higher-order n -point functions. In this appendix, we derive the Limber-approximated lensing convergence power spectrum and trispectrum expressions that we used in the main body of the paper (cf. Eqs. (4.7) and (4.8)). We also briefly comment on what is needed in order to go beyond the Limber approximation in the lensing covariance.

To warm up for the trispectrum, we derive with some care the Limber formula for the angular power spectrum of the convergence, Eq. (4.7). The lensing convergence power

spectrum is defined in the flat-sky limit as $(2\pi)^2\delta_D(\boldsymbol{\ell} + \boldsymbol{\ell}')C(\boldsymbol{\ell}) = \langle \tilde{\kappa}(\boldsymbol{\ell})\tilde{\kappa}(\boldsymbol{\ell}') \rangle$. Integrating over $d^2\boldsymbol{\ell}'$, the power spectrum can be worked out as follows:

$$\begin{aligned}
C(\boldsymbol{\ell}) &= \int \frac{d^2\boldsymbol{\ell}'}{(2\pi)^2} \langle \tilde{\kappa}(\boldsymbol{\ell})\tilde{\kappa}(\boldsymbol{\ell}') \rangle \\
&= \int \frac{d^2\boldsymbol{\ell}'}{(2\pi)^2} \int d^2\boldsymbol{\theta}_1 d^2\boldsymbol{\theta}_2 \langle \kappa(\boldsymbol{\theta}_1)\kappa(\boldsymbol{\theta}_2) \rangle e^{i\boldsymbol{\ell}\boldsymbol{\theta}_1} e^{i\boldsymbol{\ell}'\boldsymbol{\theta}_2} \\
&= \int \frac{d^2\boldsymbol{\ell}'}{(2\pi)^2} \int d^2\boldsymbol{\theta}_1 d^2\boldsymbol{\theta}_2 \int d\chi_1 d\chi_2 g(\chi_1)g(\chi_2) \langle \delta(\chi_1\boldsymbol{\theta}_1, \chi_1)\delta(\chi_2\boldsymbol{\theta}_2, \chi_2) \rangle e^{i\boldsymbol{\ell}\boldsymbol{\theta}_1} e^{i\boldsymbol{\ell}'\boldsymbol{\theta}_2} \\
&= \int \frac{d^2\boldsymbol{\ell}'}{(2\pi)^2} \int d^2\boldsymbol{\theta}_1 d^2\boldsymbol{\theta}_2 \int d\chi_1 d\chi_2 g(\chi_1)g(\chi_2) \int \frac{d^3\mathbf{k}}{(2\pi)^3} P_m(\mathbf{k}, \chi_1, \chi_2) \\
&\quad \times e^{-i\mathbf{k}_\perp(\chi_1\boldsymbol{\theta}_1 - \chi_2\boldsymbol{\theta}_2)} e^{-ik_\parallel(\chi_1 - \chi_2)} e^{i\boldsymbol{\ell}\boldsymbol{\theta}_1} e^{i\boldsymbol{\ell}'\boldsymbol{\theta}_2} \\
&= \int d^2\boldsymbol{\theta}_1 \int d\chi_1 d\chi_2 g(\chi_1)g(\chi_2) \int \frac{d^3\mathbf{k}}{(2\pi)^3} P_m(\mathbf{k}, \chi_1, \chi_2) e^{-ik_\parallel(\chi_1 - \chi_2)} e^{i\boldsymbol{\theta}_1(\boldsymbol{\ell} - \mathbf{k}_\perp\chi_1)} \\
&= \int d\chi_1 d\chi_2 \frac{g(\chi_1)}{\chi_1^2} g(\chi_2) \int \frac{dk_\parallel}{2\pi} P_m\left(\mathbf{k} = \left(\frac{\boldsymbol{\ell}}{\chi_1}, k_\parallel\right), \chi_1, \chi_2\right) e^{-ik_\parallel(\chi_1 - \chi_2)}
\end{aligned} \tag{C.1}$$

In the second equality we have written down the inverse Fourier transformed $\tilde{\kappa}$; in the third equality we have used the definition of the convergence as a weighted density projection, Eq. (4.1); in the fourth equality we have expanded the density in real space into Fourier modes, used the definition of the unequal-time matter power spectrum $(2\pi)^3\delta(\mathbf{k} + \mathbf{k}')P_m(\mathbf{k}, \chi_1, \chi_2) = \langle \delta(\mathbf{k}, \chi_1)\delta(\mathbf{k}', \chi_2) \rangle$, and integrated over $d^3\mathbf{k}'$ using the Dirac-delta function; in the fifth equality, we used that the integration over $d^2\boldsymbol{\ell}'$ yields $\delta_D(\boldsymbol{\theta}_2)$ to integrate over $d^2\boldsymbol{\theta}_2$; finally, in the last equality, we used that the integration over $d^2\boldsymbol{\theta}_1$ yields a Dirac-delta $\delta_D(\boldsymbol{\ell} - \mathbf{k}_\perp\chi_1)$ to integrate over $d^2\mathbf{k}_\perp$, which sets $\mathbf{k}_\perp = \boldsymbol{\ell}/\chi_1$ with $\mathbf{k} = (\mathbf{k}_\perp, k_\parallel)$.

The Limber approximation assumes that if one is interested in sufficiently small angular scales (large ℓ), then the dependence of the power spectrum on k_\parallel can be neglected. This is because the contribution from modes $k_\parallel \gtrsim 1/\chi$ (where χ here denotes the typical line-of-sight distances involved) is suppressed by the oscillations of the integrand. If we are then interested in cases of large ℓ , then $\ell/\chi \gg k_\parallel$ and we can set $\mathbf{k} \approx (\boldsymbol{\ell}/\chi, 0)$ in the argument of the power spectrum in Eq. (C.1). Doing so, the integral over dk_\parallel yields a Dirac-delta $\delta_D(\chi_1 - \chi_2)$, and therefore we arrive at the result of Eq. (4.7):

$$C(\boldsymbol{\ell}) = \int d\chi [g(\chi)]^2 \chi^{-2} P_m\left(\mathbf{k} = \frac{\boldsymbol{\ell}}{\chi}; z(\chi)\right). \tag{C.2}$$

For the case of the trispectrum, the derivation is analogous to that of the power spectrum, just with a larger number of integrals. In the flat-sky limit, the convergence trispectrum can be written as

$$(2\pi)^2\delta_D(\boldsymbol{\ell}_{abcd})\mathcal{T}_\kappa(\boldsymbol{\ell}_a, \boldsymbol{\ell}_b, \boldsymbol{\ell}_c, \boldsymbol{\ell}_d) = \langle \tilde{\kappa}(\boldsymbol{\ell}_a)\tilde{\kappa}(\boldsymbol{\ell}_b)\tilde{\kappa}(\boldsymbol{\ell}_c)\tilde{\kappa}(\boldsymbol{\ell}_d) \rangle, \tag{C.3}$$

from which it follows that

$$\begin{aligned} \mathcal{T}(\ell_a, \ell_b, \ell_c, -\ell_{abc}) &= \int \frac{d^2 \ell_d}{(2\pi)^2} \left[\prod_{m=a,b,c,d} \int d^2 \theta_m \int d\chi_m g(\chi_m) e^{i\ell_m \theta_m} \int \frac{d^3 \mathbf{k}_m}{(2\pi)^{12}} \right. \\ &\quad \left. \times e^{-i\mathbf{k}_{m,\perp} \theta_m \chi_m} e^{-ik_{m,\parallel} \chi_m} \right] \\ &\quad \times \langle \tilde{\delta}(\mathbf{k}_a, \chi_a) \tilde{\delta}(\mathbf{k}_b, \chi_b) \tilde{\delta}(\mathbf{k}_c, \chi_c) \tilde{\delta}(\mathbf{k}_d, \chi_d) \rangle. \end{aligned} \quad (\text{C.4})$$

Using the definition of the three-dimensional matter trispectrum, integrating over $d^3 \mathbf{k}_d$, and further integrating over $d^2 \ell_d$ yields $\delta_D(\theta_d)$, which fixes $\theta_d = 0$ after integrating over $d^2 \theta_d$. We can thus write

$$\begin{aligned} \mathcal{T}_\kappa(\ell_a, \ell_b, \ell_c, -\ell_{abc}) &= \\ &= \left[\prod_{m=a,b,c,d} \int d\chi_m g(\chi_m) \right] \left[\prod_{n=a,b,c} \int d^2 \theta_n \int \frac{d^3 \mathbf{k}_n}{(2\pi)^9} e^{i\theta_n(\ell_n - \mathbf{k}_{n,\perp} \chi_n)} e^{-ik_{n,\parallel}(\chi_n - \chi_d)} \right] \\ &\quad \times T^{\text{uneq.}}(\mathbf{k}_a, \mathbf{k}_b, \mathbf{k}_c, -\mathbf{k}_{abc}) \\ &= \left[\prod_{m=a,b,c,d} \int d\chi_m \frac{g(\chi_m)}{\chi_a^2 \chi_b^2 \chi_c^2} \right] \left[\prod_{n=a,b,c} \int \frac{dk_{\parallel,n}}{(2\pi)^3} e^{-ik_{n,\parallel}(\chi_n - \chi_d)} \right] \\ &\quad \times T^{\text{uneq.}} \left(\left(\frac{\ell_a}{\chi_a}, k_{a,\parallel} \right), \left(\frac{\ell_b}{\chi_b}, k_{b,\parallel} \right), \left(\frac{\ell_c}{\chi_c}, k_{c,\parallel} \right), \left(-\frac{\ell_a}{\chi_a} - \frac{\ell_b}{\chi_b} - \frac{\ell_c}{\chi_c}, -k_{abc,\parallel} \right) \right), \end{aligned} \quad (\text{C.5})$$

where in the second equality, we have used that the integrations over $d^2 \theta_n$ yield $\delta_D(\ell_n - \mathbf{k}_{n,\perp} \chi_n)$ Dirac-delta functions, which then fix the transverse part of the Fourier modes \mathbf{k}_n as $\mathbf{k}_{n,\perp} = \ell_n / \chi_n$ after integrating over $d^2 \mathbf{k}_{n,\perp}$. To ease the notation above, we have skipped writing the χ_n dependence on the unequal-time matter trispectrum, but added the superscript uneq. to call attention to it. As for the case of the power spectrum, the Limber approximation amounts to setting $k_{n,\parallel} = 0$ in the trispectrum arguments. Doing so, the integrals over $dk_{n,\parallel}$ yield $\delta_D(\chi_n - \chi_d)$ Dirac-delta functions, which upon integration over $d\chi_n$ allows us to arrive at Eq. (4.8):

$$\mathcal{T}(\ell_a, \ell_b, \ell_c, \ell_d) = \int d\chi [g(\chi)]^4 \chi^{-6} T_m \left(\frac{\ell_a}{\chi}, \frac{\ell_b}{\chi}, \frac{\ell_c}{\chi}, \frac{\ell_d}{\chi}; z(\chi) \right). \quad (\text{C.6})$$

The validity of the Limber and flat-sky approximations in power spectra calculations is well documented and understood (see e.g. Refs. [58–61]). To the best of our knowledge, the same level of understanding is however currently absent for the case of the trispectrum. To go beyond these approximations in the weak lensing convergence power spectrum covariance, one needs a full description of the unequal-time matter trispectrum for general configurations, i.e. not restricted to the covariance configuration. Moreover, a separation of the weak lensing covariance into cNG and SSC contributions is in general not possible beyond the Limber approximation. Finally, the numerical evaluation requires multi-dimensional integrals with oscillating integrands (see e.g. Ref. [62]), which presumably partly explains why such calculations have never been carried out (see also Ref. [63] for the full lensing bispectrum equations). These developments are beyond the scope of this paper, but we note that the validity of the Limber and flat-sky approximations should eventually be checked for the trispectrum as well, especially in light of the unprecedented statistical precision expected from upcoming wide-field lensing surveys such as Euclid [64], LSST [65] and WFIRST [66].

References

- [1] E. Sellentin and A. F. Heavens, MNRAS **456**, L132 (2016), [[arXiv:1511.05969](#)].
- [2] E. Sellentin and A. F. Heavens, ArXiv e-prints (2017), [[arXiv:1707.04488](#)].
- [3] S. Alam *et al.*, MNRAS **470**, 2617 (2017), [[arXiv:1607.03155](#)].
- [4] J. N. Grieb *et al.*, MNRAS **467**, 2085 (2017), [[arXiv:1607.03143](#)].
- [5] A. G. Sánchez *et al.*, MNRAS **464**, 1640 (2017), [[arXiv:1607.03147](#)].
- [6] H. Hildebrandt *et al.*, MNRAS **465**, 1454 (2017), [[arXiv:1606.05338](#)].
- [7] S. Joudaki *et al.*, ArXiv e-prints (2017), [[arXiv:1707.06627](#)].
- [8] E. van Uitert *et al.*, ArXiv e-prints (2017), [[arXiv:1706.05004](#)].
- [9] E. Krause *et al.*, ArXiv e-prints (2017), [[arXiv:1706.09359](#)].
- [10] DES Collaboration *et al.*, ArXiv e-prints (2017), [[arXiv:1708.01530](#)].
- [11] R. Scoccimarro, M. Zaldarriaga and L. Hui, APJ **527**, 1 (1999), [[arXiv:astro-ph/9901099](#)].
- [12] M. Takada and B. Jain, MNRAS **395**, 2065 (2009), [[arXiv:0810.4170](#)].
- [13] D. Bertolini, K. Schutz, M. P. Solon and K. M. Zurek, JCAP **6**, 052 (2016), [[arXiv:1604.01770](#)].
- [14] D. Bertolini, K. Schutz, M. P. Solon, J. R. Walsh and K. M. Zurek, Phys. Rev. D **93**, 123505 (2016), [[arXiv:1512.07630](#)].
- [15] A. Barreira and F. Schmidt, JCAP **6**, 053 (2017), [[arXiv:1703.09212](#)].
- [16] A. Barreira and F. Schmidt, ArXiv e-prints (2017), [[arXiv:1705.01092](#)].
- [17] M. Takada and W. Hu, Phys.Rev. D **87**, 123504 (2013), [[arXiv:1302.6994](#)].
- [18] Y. Li, W. Hu and M. Takada, Phys. Rev. D **89**, 083519 (2014), [[arXiv:1401.0385](#)].
- [19] Y. Li, W. Hu and M. Takada, Phys. Rev. D **90**, 103530 (2014), [[arXiv:1408.1081](#)].
- [20] A. Manzotti, W. Hu and A. Benoit-Lévy, PRD **90**, 023003 (2014), [[arXiv:1401.7992](#)].
- [21] M. Takada and D. N. Spergel, MNRAS **441**, 2456 (2014), [[arXiv:1307.4399](#)].
- [22] R. Takahashi, S. Soma, M. Takada and I. Kayo, MNRAS **444**, 3473 (2014), [[arXiv:1405.2666](#)].
- [23] C. Wagner, F. Schmidt, C.-T. Chiang and E. Komatsu, Mon.Not.Roy.Astron.Soc. **448**, 11 (2015), [[arXiv:1409.6294](#)].
- [24] Y. Li, W. Hu and M. Takada, Phys. Rev. D **93**, 063507 (2016), [[arXiv:1511.01454](#)].
- [25] T. Baldauf, U. Seljak, L. Senatore and M. Zaldarriaga, JCAP **9**, 007 (2016), [[arXiv:1511.01465](#)].
- [26] C. Wagner, F. Schmidt, C.-T. Chiang and E. Komatsu, JCAP **8**, 042 (2015), [[arXiv:1503.03487](#)].
- [27] C.-T. Chiang, A. M. Cieplak, F. Schmidt and A. Slosar, ArXiv e-prints (2017), [[arXiv:1701.03375](#)].
- [28] F. Bernardeau, S. Colombi, E. Gaztañaga and R. Scoccimarro, Phys. Rep. **367**, 1 (2002), [[arXiv:astro-ph/0112551](#)].
- [29] L. Dai, E. Pajer and F. Schmidt, JCAP **10**, 059 (2015), [[arXiv:1504.00351](#)].
- [30] T. Lazeyras, C. Wagner, T. Baldauf and F. Schmidt, JCAP **2**, 018 (2016), [[arXiv:1511.01096](#)].
- [31] D. Bertolini and M. P. Solon, JCAP **11**, 030 (2016), [[arXiv:1608.01310](#)].
- [32] L. Blot, P. S. Corasaniti, J.-M. Alimi, V. Reverdy and Y. Rasera, MNRAS **446**, 1756 (2015), [[arXiv:1406.2713](#)].

- [33] A. J. S. Hamilton, C. D. Rimes and R. Scoccimarro, MNRAS **371**, 1188 (2006), [[arXiv:astro-ph/0511416](#)].
- [34] E. Sefusatti, M. Crocce, S. Pueblas and R. Scoccimarro, Phys. Rev. D **74**, 023522 (2006), [[arXiv:astro-ph/0604505](#)].
- [35] R. de Putter, C. Wagner, O. Mena, L. Verde and W. J. Percival, JCAP **4**, 019 (2012), [[arXiv:1111.6596](#)].
- [36] M. Takada and S. Bridle, New Journal of Physics **9**, 446 (2007), [[arXiv:0705.0163](#)].
- [37] I. Kayo, M. Takada and B. Jain, MNRAS **429**, 344 (2013), [[arXiv:1207.6322](#)].
- [38] M. Sato *et al.*, Astrophys. J. **701**, 945 (2009), [[arXiv:0906.2237](#)].
- [39] W. Hu and A. V. Kravtsov, Astrophys. J. **584**, 702 (2003), [[arXiv:astro-ph/0203169](#)].
- [40] K. Akitsu, M. Takada and Y. Li, Phys. Rev. D **95**, 083522 (2017), [[arXiv:1611.04723](#)].
- [41] K. Akitsu and M. Takada, ArXiv e-prints (2017), [[arXiv:1711.00012](#)].
- [42] Y. Li, M. Schmittfull and U. Seljak, ArXiv e-prints (2017), [[arXiv:1711.00018](#)].
- [43] B. D. Sherwin and M. Zaldarriaga, Phys. Rev. D **85**, 103523 (2012), [[arXiv:1202.3998](#)].
- [44] M. Bartelmann and P. Schneider, PhysRep **340**, 291 (2001), [[arXiv:astro-ph/9912508](#)].
- [45] P. Schneider, ArXiv Astrophysics e-prints (2005), [[arXiv:astro-ph/0509252](#)].
- [46] H. Hoekstra and B. Jain, Annual Review of Nuclear and Particle Science **58**, 99 (2008), [[arXiv:0805.0139](#)].
- [47] M. Kilbinger, Reports on Progress in Physics **78**, 086901 (2015), [[arXiv:1411.0115](#)].
- [48] A. Petri, Z. Haiman and M. May, PRD **95**, 123503 (2017), [[arXiv:1612.00852](#)].
- [49] F. Bernardeau, C. Bonvin and F. Vernizzi, PRD **81**, 083002 (2010), [[arXiv:0911.2244](#)].
- [50] S. Dodelson, C. Shapiro and M. White, Phys. Rev. D **73**, 023009 (2006), [[arXiv:astro-ph/0508296](#)].
- [51] E. Krause and C. M. Hirata, Astronomy & Astrophysics **523**, A28 (2010), [[arXiv:0910.3786](#)].
- [52] F. Schmidt, E. Rozo, S. Dodelson, L. Hui and E. Sheldon, Astrophys. J. **702**, 593 (2009), [[arXiv:0904.4703](#)].
- [53] J. Lesgourgues, ArXiv e-prints (2011), [[arXiv:1104.2932](#)].
- [54] R. Takahashi, M. Sato, T. Nishimichi, A. Taruya and M. Oguri, Astrophys. J. **761**, 152 (2012), [[arXiv:1208.2701](#)].
- [55] F. Lacasa, M. Lima and M. Agüena, ArXiv e-prints (2016), [[arXiv:1612.05958](#)].
- [56] K. C. Chan and L. Blot, PRD **96**, 023528 (2017), [[arXiv:1610.06585](#)].
- [57] K. C. Chan, A. Moradinezhad Dizgah and J. Noreña, ArXiv e-prints (2017), [[arXiv:1709.02473](#)].
- [58] P. Simon, AAP **473**, 711 (2007), [[arXiv:astro-ph/0609165](#)].
- [59] M. Loverde and N. Afshordi, PRD **78**, 123506 (2008), [[arXiv:0809.5112](#)].
- [60] F. Schmidt, A. Vallinotto, E. Sefusatti and S. Dodelson, Phys. Rev. D **78**, 043513 (2008), [[arXiv:0804.0373](#)].
- [61] P. Lemos, A. Challinor and G. Efstathiou, JCAP **5**, 014 (2017), [[arXiv:1704.01054](#)].
- [62] F. Lacasa, ArXiv e-prints (2017), [[arXiv:1711.07372](#)].
- [63] W. Hu, PRD **62**, 043007 (2000), [[arXiv:astro-ph/0001303](#)].

- [64] R. Laureijs *et al.*, ArXiv e-prints (2011), [[arXiv:1110.3193](#)].
- [65] LSST Dark Energy Science Collaboration, ArXiv e-prints (2012), [[arXiv:1211.0310](#)].
- [66] D. Spergel *et al.*, ArXiv e-prints (2013), [[arXiv:1305.5422](#)].